

A large, abstract blue ink splash or paint blotch that covers the right side and bottom of the page, creating a dynamic, artistic background.

Advanced Practical Course Environmental Physics

**F59: Active Solute Transport in Saturated
Porous Media**

**Institute of Environmental Physics
Heidelberg University**

Philipp Kreyenberg

Version: June 2019

Safety Notes

In this practical course you are going to work in a laboratory environment that requires to follow the general laboratory regulations of the University of Heidelberg. You can find a printed version in the laboratories or at https://www.uni-heidelberg.de/md/zentral/universitaet/beschaeftigte/service/sicherheit/dokumente/laboratoriumsordnung_2018.pdf.

For your own safety, additional safety notes specific to this practical course are detailed in the following:

- You are going to work with the food grade coloring Brilliant Blue, which is nontoxic and not harmful in low doses. Nevertheless, it is a chemical substance that causes **serious eye irritation** and **may cause skin irritation** in high doses. Also it **causes damage to organs through prolonged or repeated exposure**.

The according safety precautions are:

- **Do not ingest the substance.**
- **Wear safety glasses, protective gloves, and laboratory coat.**
- **Wash hands thoroughly after handling.**

In case of eye contact rinse cautiously with water for several minutes. Remove contact lenses, if present and easy to do. Continue rinsing.

- For the illumination of the experimental setup a high intensity LED light source is used. Because of the blue light components of the emitted spectrum **do not stare into the LED light source** for prolonged times to avoid **harm to the retinal tissue**.
- The setup of the conducted experiments includes the mounting of two glass plates into a metal frame. When the assembly is not done carefully, the **glass plates could possibly shatter**. The used glass plates are made from single-pane safety glass and are only shattering into very small shards to minimize the risk of cutting injuries. Nevertheless, follow the according safety precautions:
 - **Wear safety glasses and laboratory coat.**
 - **Wear long trousers and solid footwear.**

Before you are allowed to begin with the work in the laboratories you have to sign that you took note of the the general laboratory regulations of the University of Heidelberg and the security notes given above and are going to act accordingly.

Contents

1	Introduction	1
2	Theoretical Background	3
2.1	Fluid Dynamics	3
2.1.1	Concepts	3
2.1.2	Forces	5
2.1.3	Conservation Laws	6
2.1.4	Dynamics	8
2.2	Equation of State	9
2.3	Porous Media	10
2.3.1	Natural Porous Media	10
2.3.2	Pseudo-Porous Media	11
2.4	Fluid Dynamics in Porous Media	11
2.4.1	Conservation of Mass	11
2.4.2	Conservation of Momentum	12
2.5	Fluid Dynamics in Hele-Shaw Cells	13
2.6	Solute Transport	14
2.6.1	Molecular Diffusion	15
2.6.2	Taylor-Aris Dispersion	15
2.6.3	Convection Dispersion Equation	16
2.7	Active Solute Transport	16
2.7.1	Dimensionless Formulation	18
2.7.2	Density-Driven Convection Regimes	19
2.7.3	Meaning of the Rayleigh Number	22
2.7.4	Critical Values	23
3	Experimental Setup, Methods, and Equipment	25
3.1	Experimental Setup	25
3.2	Measurement Method	27
3.3	Explanation of the Equipment	27
3.3.1	Camera	28
3.3.2	Spectrometer	29
3.3.3	Brilliant Blue	31
3.4	Explanation of the Scripts	34
3.4.1	Image Acquisition	34
3.4.2	Image Processing	39

4	Comprehension Check	43
5	The Experiments	45
5.1	Bare Cell Experiment	45
6	Evaluation	49
6.1	Qualitative evaluation of the image time series	49
6.2	Determination of the Critical Time and Wave Length	49
6.3	Detailed investigation of the Temporal Regimes	51
	Bibliography	53

1 Introduction

The transport of heat and mass through convection is a critical process to many environmental systems and leads to a plethora of interesting phenomena. Particularly when the convection is driven by density contrasts a whole set of beautiful and astonishingly similar phenomena emerge. Examples of these phenomena include morphological processes in the mantle of the earth ([Conrad and Molnar, 1997](#)), the disposal of toxic and radioactive wastes in rock salt formations ([Kolditz et al., 1998](#)), saltwater intrusion in exploited coastal aquifers ([Diersch and Kolditz, 2002](#)), and dynamics of water motion in aquifers beneath saline lakes (e.g. ([Wooding et al., 1997a](#)), ([Wooding et al., 1997b](#))).

More recently convection in porous media gained renewed attention especially with the storage of anthropogenic carbon-dioxide in deep geological brine formations (([Ennis-King et al., 2005](#)), ([Davidson and Metz, 2005](#)) and ([Riaz et al., 2006](#))). This technique is referred to as carbon-dioxide sequestration, where CO_2 is injected into 1 to 3 km deep saline aquifers under supercritical conditions. Compared to the present brine the CO_2 is positively buoyant and accumulates as a horizontally spread layer under impermeable cap rock. At the interface the supercritical CO_2 then dissolves into the brine causing an increase of the brine density there, introducing a gravitationally unstable stratification. At first the downward transport is only due to diffusion leading to a very slow process in the order of several thousand years, but eventually the situation becomes unstable and density-driven convection sets in by the formation of distinct finger like structures intruding into the pure brine. This process decreases the time scale of the transport by several orders of magnitude.

In this practical course a lab scale system that is analog to the problem of carbon-dioxide sequestration is implemented and investigated. This is possible, as the principles of fluid dynamics are applicable over a vast range of scales, as long as the investigated media fulfill the requirements to be described as a fluid. As we will see, this permits the dimensionless formulation of the governing equations, demonstrating the analog behavior of such systems.

In addition to this a goal of the course is to introduce how already simple coupling of two linear processes can lead to nonlinear behavior, exhibiting temporal regime shifts of the transport process. This is exemplified by the chosen system governed by the interplay of diffusion and convection.

With this an introduction to the wide range of phenomena with respect to convective transport and flow instabilities is given.

2 Theoretical Background

This chapter introduces mathematical models representing the main aspects to understand the process of density-driven instabilities in porous media, which is the subject of study for the practical course. For notational convenience, the general term fluids will be used, although only water and dilute aqueous solution of a solute are used in the experiments. To approach the matter we take a look at the concepts of moving fluids first, then the medium of interest and its flow domain afterwards. Therefore, first an introduction into fluid dynamics is given, then the equation of state for water with respect to the solute concentration is described before the concept of porous media characterizing natural soils is introduced. Furthermore, the governing equation of fluid dynamics are specialized for the case of fluids in porous media and is then discussed for the geometry of Hele-Shaw cells as a model for such a porous medium. Closing the set of equations for the considered problem, the description for solute transport is introduced. Finally, the combination of the previous concepts yields the theoretical basis for the density-driven instabilities in Hele-Shaw cells.

For the most part, this chapter follows the representation of [Roth \(2012\)](#) and is in parts based on [Kreyenberg \(2015\)](#).

2.1 Fluid Dynamics

In this section we introduce the principles of *fluid dynamics*, which describes the relation between forces on fluids and its motion in a continuum representation.

2.1.1 Concepts

Fluid

Fluids in this context is a very large class of systems with the following defining characteristics: (i) fluids consist of large ensembles of particles. (ii) The interaction of the particles has to be local and so weak that they are still able to move freely. (iii) Conservation of mass, linear and angular momentum, and total energy has to be fulfilled during the interactions.

Here the particles could be anything ranging from stars in galaxies to molecules in water and they are able to exhibit the same spectrum of flow phenomena, as long as the above

mentioned characteristics are fulfilled.

Continuum

To derive the description of its motion fluids are described in a continuum representation. To allow for this continuum representation the behavior of the ensemble of particles must not depend on its details, but just on some average properties. These so called macroscopic properties are calculated by the appropriate averages over the ensemble of the particles. As an example, consider the number of air molecules $n(r)$ contained in the volume of a small sphere around location \mathbf{x} with radius r and their respective velocities \mathbf{v}^μ . The average velocity of the ensemble is then given by:

$$\mathbf{v}_r(x) = \langle \mathbf{v}^\mu \rangle_r = \frac{1}{n(r)} \sum_{i=1}^{n(r)} \mathbf{v}_i^\mu, \quad (2.1)$$

where the superscript μ denotes the microscopic perspective of the particles. For the case of a small r , variations of r and \mathbf{x} both lead to strong fluctuations in \mathbf{v}_r . With increasing r this fluctuation decreases and ideally vanishes, leading to an objective value for \mathbf{v}_r , which then represents the velocity $\mathbf{v}(\mathbf{x}, t)$ at the continuum or macroscopic scale. The averaging volume that supports this objective value $\mathbf{v}(\mathbf{x}, t)$ is called the *representative elementary volume* (REV). This REV does not necessarily have the shape of a sphere and could be shaped arbitrarily in general, as long as the averaging leads to the macroscopic quantity. Analog with the example of the velocity, also other quantities are defined with the respective REV.

In conclusion, we find that the existence of the REV has to be given to allow for the macroscopic representation of the fluid. In environmental physics this is given almost always, since the considered fluids are comparatively dense. For example, the volume of $1 \mu\text{m}^3$ of liquid water contains around $3.3 \cdot 10^{10}$ molecules. Therefore the averaging extends over a huge number of particles, even at rather small scales, and guarantees the existence of a REV.

Fluid Element

Since fluid dynamics is formulated in a continuum representation it is convenient to introduce a fluid element, which is a *mass element* that moves and deforms with the fluid flow and extends over a volume V with surface ∂V that is at least of the size of the REV. For better imagination, we can think of an ensemble of tagged particles for which integrating and/or averaging leads to the properties of the fluid element (mass, momentum, kinetic and thermal energy, ...). Since neighboring particles experience similar forces, they stay neighboring for quite some time.

When looking at the forces acting on the fluid element, due to Newton's third law - action equals reaction - all the short-range forces within the fluid element and within the sur-

rounding fluid balance each other and cancel out in total. But two types of forces acting on the fluid element as a whole are left. The first kind are the long-range body forces, for instance gravity. The second kind are short-range surface forces like the van der Waals forces between particles outside of the fluid element and the those within, which lead to net forces on the surface ∂V with a normal component as well as shear components. These surface forces are the reason for the compression or expansion and the deformation of the fluid element with time.

The forces between particles within the fluid element and within the surrounding fluid are represented by material properties, in particular the compressibility and the viscosity, when considering the continuum perspective.

2.1.2 Forces

Consider a fluid element and the various external forces acting on it. As introduced above, there are the long-range body forces \mathbf{f}_b and the short-range surface forces \mathbf{f}_s .

Body forces

The most prominent body force in the context of this course is Gravity. In an external gravitational field g the force exerted on the fluid element is given by:

$$\mathbf{F}_g = \int_V \mathbf{g} \rho dV \quad (2.2)$$

with the mass density ρ .

Surface forces

In contrast to body forces, the short-range surface forces are more complicated to deal with. By invoking Newton's second law, $\mathbf{F} = \dot{\mathbf{p}}$, for the particles at the fluid elements' surface ∂V and by recognizing that a force per unit area corresponds to a momentum flux across this area, we can derive the resulting surface forces. The *momentum flux* \mathbf{J} , a tensorial quantity, consists of the components J_{ij} , which are the respective fluxes of i -momentum flowing in j -direction. The separation of the normal and shear contribution of the tensor result in:

$$J_{ij} = p\delta_{ij} + \Pi_{ij}, \quad (2.3)$$

where δ_{ij} is Kronecker's delta and Π_{ij} is a component of the so-called *viscous momentum flux tensor* Π . Therefore, the pressure, given by the normal part, is leading to compression

of the fluid element without any deformation. The shear part corresponds to friction being responsible for deformation without changing the absolute volume of the fluid element.

Pressure The pressure force acting on the fluid element's surface is given by

$$\mathbf{F}_p = - \int_{\partial V} p \, d\mathbf{A} = - \int_V \nabla p \, dV, \quad (2.4)$$

with the sign accounting for the convention of outwards pointing normal vector $d\mathbf{A}$. In the second equality the Gauss' theorem was applied.

Friction The viscous force on the fluid element can be calculated by integrating the viscous momentum flow $\Pi d\mathbf{A}$ over the surface of the fluid element ∂V . This yields the total inflow of momentum per unit time and therefore determines the rate with which the fluid element's momentum changes. The viscous force acting on the surface of the fluid element is then given by

$$\mathbf{F}_v = - \int_{\partial V} \Pi \, d\mathbf{A} = - \int_V [\nabla \Pi] \, dV, \quad (2.5)$$

again with the sign accounting for the outwards pointing normal vector $d\mathbf{A}$ and Gauss' theorem being applied to the second equality.

Assuming the simpler case of an incompressible Newtonian fluid, which often holds in environmental systems, it can be shown that the viscous force is given by

$$\mathbf{F}_v = \mu \int_V \nabla^2 \mathbf{v} \, dV, \quad (2.6)$$

with $\mu[\text{Pas}]$ being the dynamic viscosity of the fluid.

Having understood the differences between body forces and surface forces acting on the fluid element, we turn our attention to the formulation of the conservation laws for the fluid flow.

2.1.3 Conservation Laws

To formulate the conservation laws we choose either the Eulerian or the Lagrangian perspective. In the Eulerian perspective we observe a volume fixed in space and consider the net inflow of the conserved quantity and relate it to the temporal change of that quantity within the volume. In contrast to this there is the Lagrangian perspective, where a fluid element is followed in its motion along with the evaluation of the inflow and rate of change of the conserved quantity within the fluid element. For the situations encountered

within this practical course it is sufficient to introduce the conservation of mass and linear momentum.

Conservation of Mass

For the formulation of the conservation of mass we choose the Eulerian framework. Here, the rate of change of mass within the volume V is given by the mass flow across its surface ∂V :

$$\underbrace{\partial_t \int_V \rho \, dV}_{\text{mass in } V} = - \underbrace{\int_{\partial V} [\rho \mathbf{v}] \cdot d\mathbf{A}}_{\text{mass flow into } V} = - \int_V \nabla \cdot [\rho \mathbf{v}] \, dV, \quad (2.7)$$

again with the sign because of outwards pointing $d\mathbf{A}$ and Gauss' theorem being applied to the second equality. Since the volume V is arbitrarily chosen, we conclude the general form of the conservation of mass:

$$\partial_t \rho + \nabla \cdot [\rho \mathbf{v}] = 0. \quad (2.8)$$

For an incompressible and pure fluid this means $\rho = \text{const}$ and (2.8) simplifies further to

$$\nabla \cdot \mathbf{v} = 0. \quad (2.9)$$

Conservation of Momentum

Because it makes it easier we choose the Lagrangian perspective to formulate the conservation of momentum. With the velocity \mathbf{v} of the fluid element's center of gravity the momentum is given by

$$m\mathbf{v} = \left[\int_V \rho \, dV \right] \mathbf{v}. \quad (2.10)$$

Therefore, the rate of change of linear momentum is given by $m d_t \mathbf{v}$, since the mass of the fluid element is constant by definition. According to Newton's second law the rate of change of linear momentum equals the sum of the previously introduced body and surface forces, (2.2), (2.4), and (2.6). This leads to:

$$\left[\int_V \rho \, dV \right] d_t \mathbf{v} = \mathbf{F}_g + \mathbf{F}_p + \mathbf{F}_v = \int_V [\rho \mathbf{g} - \nabla p - \mu \nabla^2 \mathbf{v}] \, dV. \quad (2.11)$$

Again the volume of the fluid element V is chosen arbitrarily and we can conclude the general conservation of linear momentum:

$$\rho d_t \mathbf{v} = \rho \partial_t \mathbf{v} + \rho [\mathbf{v} \cdot \nabla] \mathbf{v} = \rho \mathbf{g} - \nabla p - \mu \nabla^2 \mathbf{v}. \quad (2.12)$$

This equation is the *Navier Stokes equation*, which is, as given above, the general description for linear momentum of any incompressible and isotropic Newtonian fluid. Taking a look at the inertia term in this equation:

$$[\mathbf{v} \cdot \nabla] \mathbf{v} = [\mathbf{v} \times \nabla] \times \mathbf{v} - \frac{1}{2} \nabla v^2, \quad (2.13)$$

where the nonlinearity of the Navier Stokes equation becomes apparent reveals its challenges. This nonlinearity causes trouble in finding a general analytic solution and is quite impossible with current methods. There is not even a proof yet that a smooth solution always does exist for three dimensional flow. As an aside, this proof is one of the *Millennium Prize* problems in mathematics announced by the *Clay Mathematics Institute*. For a further introduction into the characteristics of the Navier Stokes equation see ([Roth, 2012](#)) and ([Roth, 2016](#)).

For the application purposes of this course we are using a simplification of the Navier Stokes equation. For slow characteristic flow velocities and small characteristic length scales of the flow domain it can be shown that the inertia term can be neglected and we end up with the *time-dependent Stokes equation*:

$$\rho \partial_t \mathbf{v} = \rho \mathbf{g} - \nabla p - \mu \nabla^2 \mathbf{v}. \quad (2.14)$$

In this course we deal only with slow flow and porous media, and therefore are only interested in this simplified formulation.

2.1.4 Dynamics

With these conservation laws we essentially formulated the dynamics of a fluid. Taking several assumptions to simplify the equations into account this summarizes to

$$\nabla \cdot \mathbf{v} = 0 \quad (2.15)$$

$$\rho \partial_t \mathbf{v} = \rho \mathbf{g} - \nabla p - \mu \nabla^2 \mathbf{v} \quad (2.16)$$

for an incompressible, pure, and Newtonian fluid. When these assumptions can not be made, the more general form of the respective equation has to be consulted. Independent of the choice of generality for the dynamics we find that this formulation is not sufficient to describe the fluid flow uniquely. This is because with (2.16) and (2.16) we have 4

equations to describe 5 unknown fields (ρ, \mathbf{v}, p) . To resolve this issue we introduce the *equation of the state* for the fluid of interest as described in the following section. With this the unknown fields are reduced to \mathbf{v} and p .

2.2 Equation of State

As water or dilute aqueous dye solutions are the fluids of interest within the scope of this practical course, the equation of state of water is presented in the following. Generally one considers the thermodynamic relations for the internal energy U and the density ρ . However, the presentation of the relation for the internal energy U is omitted here, since all experiments are conducted with a constant and homogeneous temperature distribution. In contrast the density is important for the following considerations as it generally depends on the pressure p , the concentration of solute C , and the temperature T . In the special case relevant to the conducted studies the following assumptions can be made: T is constant and the water is incompressible throughout the used flow domains, since its spatial extent is small. Hence, the total differential of the density ρ is:

$$d\rho = \underbrace{\frac{1}{\rho} \frac{\partial \rho}{\partial C}}_{\beta} \cdot \rho dC, \quad (2.17)$$

where $\beta > 0$ is the volumetric *solotal expansion coefficient*, which is assumed to be constant for small changes in C . The relation describes the infinitesimal increase in density $d\rho$, due to an infinitesimal increase in solute concentration dC . This leads to the simplified equation of state of water:

$$\rho(C) = \rho_0 \cdot \exp(\beta(C - C_0)). \quad (2.18)$$

Linear approximation yields:

$$\rho(C) = \rho_0 + \beta'(C - C_0). \quad (2.19)$$

Here, ρ_0 and C_0 are suitable reference values for the density and the solute concentration and β' is given by $\beta' = \rho_0 \beta$. The linear approximation is considered to be valid, as the variations of the concentrations are small.

In the case of unknown *solotal expansion coefficient*, it is useful to consider a different approach of linear approximation of the equation of state:

$$\rho(c) = \rho_1 + (\rho_2 - \rho_1) \cdot c, \quad (2.20)$$

with the reduced concentration:

$$c = \frac{(C - C_0)}{(C_{\max} - C_0)}; \quad c \in [0, 1]. \quad (2.21)$$

Equation (2.20) describes the linear interpolation between the maximum density $\rho_{\max}(C_{\max})$ and the minimum density $\rho_0(C_0)$ found in the particular situation. Again, this approximation is valid for small variations in C . For these small variations the viscosity μ of the water is considered to be constant.

This closes the description of fluid dynamics as far as we need it to understand the conducted experiments. In the following we turn out focus on the flow domain of porous media to be able to merge the concepts and to look at fluid dynamics in porous media.

2.3 Porous Media

As the term porous media generally covers a wide range of geometric arrangements, this section introduces some aspects of natural porous media important in soils. In particular the formal correspondence between Hele-Shaw cells and porous media is presented.

2.3.1 Natural Porous Media

A porous medium is in universal description a medium that consists of voids of any arbitrary shape embedded in a matrix. In the case of natural porous media, with respect to soils, the voids are represented by pores and the matrix is represented by grains or particles of the solid material (*Nield and Bejan, 1999*). The volume fraction of pores defines porosity ϕ :

$$\phi := \frac{V_{\text{pore}}}{V_{\text{tot}}} \quad (2.22)$$

with V_{pore} being the volume of the pores embedded in the total volume V_{tot} of the porous medium. Another important property of a porous medium representing soils is the interconnectedness of pores enabling fluids to flow through the soil. The grains or particles creating the matrix are of various sizes and typically have a rough surface, whereat the grain sizes could extend over a wide range. Examples for the porosity of natural soils are $\phi = 0.32$ (sand) and $\phi = 0.41$ (silt) (*Van Dam et al., 1992*), where spaces between larger grains are filled with smaller particles.

It shall be noted that the prior definition of ϕ only holds for the case of interconnected pores. If some pores are isolated from the interconnected pore space, an effective porosity has to be introduced describing the actual fluid flow. The effective porosity is defined as the ratio between connected pore space and total volume of the porous medium.

This summarizes the most important characteristics of natural porous media prerequisite to understanding the differences and similarities to Hele-Shaw cells. A far more detailed description of porous media in the context of natural soils is given in *Roth (2012)*.

2.3.2 Pseudo-Porous Media

In contrast to natural porous media a class of pseudo-porous media can be specified. The members of this class show the same, or at least similar, behavior for fluid flows within their pore space, but lack of one or more aspects to describe a full natural porous medium. In this sense pseudo-porous media are models aiding to understand the dynamics of fluid flow in natural porous media.

One example of such a pseudo-porous medium is a Hele-Shaw cell, which consists of two plane glass plates with a small gap of width d in between. For Hele-Shaw cells the extent of the glass plates is usually much larger than the small gap to create a lateral extended flow domain. The key-idea of Hele-Shaw cells is to represent one large pore that simulates a porous medium and the flow within. Since the cells consist of glass the fluid motion in the gap is directly observable and can be investigated. On the other side, the way they are constructed already indicate the limitation of Hele-Shaw cells to represent a natural porous medium. Since there is only one large pore and no matrix between the plates, the porosity satisfies $\phi = 1$. Another restriction is that Hele-Shaw cells just allow two dimensional fluid flow.

2.4 Fluid Dynamics in Porous Media

To describe the fluid dynamics in porous media it is conventional to describe the flow at a spatial average, similar to the averaging for the formulation of the continuum scale for the description of fluids. This characterizes a macroscopic scale, and not the detailed flow at the pore or microscopic scale and also requires the existence of a *representative elementary volume* (REV) as averaging volume. Here, the REV has to fulfill, at least, the following requirements: The length scale of the REV has to be much larger than the pore scale and much smaller than the macroscopic flow domain. Further, the result of the averaging has to be independent of the actual size of the REV.

In the following, the equations of fluid flow in porous media at the macroscopic scale are presented, which are accepted to model the underlying physical processes. Additionally it should be noted that only the case of completely saturated porous media is considered here. This means that all the pores are filled with just one fluid, which represents single phase fluid flow.

2.4.1 Conservation of Mass

The conservation of the fluid mass at the macroscopic scale is deduced by spatially averaging the mass balance of the fluid contained within a volume element of porous medium and its flux over the pores at the boundary. Here, the volume element has to be sufficiently large to contain many pores. This yields the macroscopic mass balance, which is given by the *continuity equation*:

$$\phi \frac{\partial \rho_w}{\partial t} + \nabla \cdot (\rho_w \mathbf{j}_w) = 0. \quad (2.23)$$

Here ρ_w is the density of water contained in the pores and \mathbf{j}_w is the macroscopic flux of water in the porous medium. The flux \mathbf{j}_w is related to the averaged intrinsic fluid velocity \mathbf{v}_w in the pores by the *Dupuit-Forchheimer relation* ([Nield and Bejan, 1999](#)):

$$\mathbf{j}_w = \phi \cdot \mathbf{v}_w. \quad (2.24)$$

Further in the above formulation of the *continuity equation* it is assumed that the porosity ϕ is constant over time and any sources or sinks are omitted.

Using the *Boussinesq-Oberbeck approximation*, equation (2.23) can be simplified to:

$$\nabla \cdot \mathbf{j}_w = 0, \quad (2.25)$$

since the variation of the density ρ_w can be neglected unless it is coupled with the acceleration of gravity \mathbf{g} . This approximation is only valid, if the variation of the density is small compared to the absolute density of the fluid, as it is found in the conducted experiments.

2.4.2 Conservation of Momentum

The fluid flow must satisfy the conservation of momentum. For porous media this involves a simplified *Stokes equation*, since the fluid flow is typically very slow and the fluid is assumed to be incompressible. Additionally, the external forcing is often encountered to be so slow to justify the assumption of a stationary flow. Again considering the complex flow domain of the fluid phase in the porous medium and averaging over the appropriate REV gives the relation for the macroscopic quantities and yields the empirical flux law named after Darcy. For a detailed discussion see [Roth \(2012\)](#).

Darcy's Law

The *Darcy's law* relates the macroscopic flux \mathbf{j}_w to the macroscopic driving forces as:

$$\mathbf{j}_w = -\frac{1}{\mu} \mathbf{k} (\nabla p - \rho_w \mathbf{g}) \quad (2.26)$$

with the dynamic viscosity μ , the permeability \mathbf{k} and the macroscopic pressure gradient ∇p . Here the permeability \mathbf{k} is generally a symmetric second rank tensor. For isotropic porous media it reduces to the scalar quantity k .

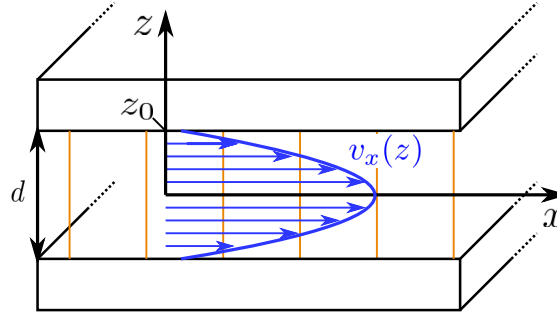


Figure 2.1: Illustration of the velocity profile $v_x(z)$ (blue line and arrows) of *Hagen-Poiseuille* flow between two parallel plates with distance d . The velocity profile is only shown in the plane of the cross section. Orange lines indicate isolines of the large scale pressure field. Figure from [Kreyenberg \(2015\)](#).

2.5 Fluid Dynamics in Hele-Shaw Cells

As mentioned in section 2.3.2, Hele-Shaw cells differ from natural porous media in two aspects: (i) They only simulate two dimensional porous media and (ii) their porosity is given by $\phi = 1$. By the virtue of the *Dupuit-Forchheimer relation* (2.24), the averaged intrinsic velocity \mathbf{v}_w and the macroscopic volume flux \mathbf{j}_w are identical for Hele-Shaw flows. Apart from this, flows in Hele-Shaw cells are described by the same relations introduced in section 2.4.

Conservation of Mass

The continuity equation for Hele-Shaw flow specializes to:

$$\frac{\partial \rho_w}{\partial t} + \nabla \cdot (\rho_w \mathbf{v}_w) = 0 \quad (2.27)$$

and, using again the *Boussinesq-Oberbeck approximation*, in simplified form to:

$$\nabla \cdot \mathbf{v}_w = 0. \quad (2.28)$$

Fluid Flow Between Two Parallel Plates

The flow of water between two parallel plates with a small gap in between can be deduced by considering the plates arranged in a horizontal configuration with a large lateral extent compared to the gap width d as illustrated in Figure 2.1. Since, for Hele-Shaw cells, the gap between the walls is very small, the simplified *Stokes equation* holds for slow flow velocities:

$$\mu \nabla^2 \mathbf{v} = \nabla p. \quad (2.29)$$

Here, the influence of gravitational forces is omitted to keep the problem as simple as possible. Nevertheless, the general conclusion of the result is not restricted and other forces could easily be introduced.

Following along the lines of [Roth \(2012\)](#), deducing the velocity profile in a long cylindrical tube, the velocity profile between the plates is deduced to be the *Hagen-Poiseuille profile* and takes parabolic form (cf. Figure [2.1](#)):

$$v_x(z) = -\frac{1}{2\mu} \frac{\partial p}{\partial x} (z_0^2 - z^2). \quad (2.30)$$

Here z_0 is the vertical distance between the center plane and the walls. This solution was derived assuming a large scale stationary pressure gradient being parallel to x . Averaging of the solution ([2.30](#)) over a cross section in the y, z -plane yields the average volume flux:

$$j_w = -\frac{d^2}{12 \cdot \mu} \frac{\partial p}{\partial x}. \quad (2.31)$$

Comparison with equation ([2.26](#)) shows that this is a simplified form of the *Darcy's law* for isotropic media and the permeability k for Hele-Shaw cells can easily be recognized as $k = d^2/12$, which has a quadratic dependence on the gap width d between the walls of the cell. This result is also applicable, if gravitational forces are present and therefore this result also holds for vertically arranged Hele-Shaw cells.

In summary it can be established that the volume flux in a Hele-Shaw cell is described by the *Darcy's law* for the special case of porosity $\phi = 1$ and permeability $k = d^2/12$. Including again gravitational forces and invoking the *Dupuit-Forchheimer* relation ([2.24](#)) the *Darcy's law* for Hele-Shaw cells reads:

$$\mathbf{v} = -\frac{d^2}{12 \cdot \mu} (\nabla p - \rho_w \mathbf{g}) \quad (2.32)$$

with \mathbf{v} being the averaged intrinsic fluid velocity and d being the gap width between the plates of the cell.

2.6 Solute Transport

To understand the transport of substances dissolved in the fluid contained in the porous medium it is important to understand the transport of the solutes within the fluid phase. This transport is affected by three mechanisms, namely, molecular diffusion, dispersion, and convection.

2.6.1 Molecular Diffusion

Molecular diffusion is solute transport at a molecular level. It is the undirected random walk of the molecules due to *Brownian motion*, counteracting any given concentration gradient and operating without any movement of the fluid. A model to describe molecular diffusion in fluids are *Fick's laws* ([Fick, 1855](#)), which are given as *Fick's first law* that relates the flux of solute mass \mathbf{j}_s to the concentration gradient ∇C :

$$\mathbf{j}_s = -D_m \nabla C \quad (2.33)$$

with the molecular diffusion coefficient D_m . *Fick's second law* combines the first law with the conservation of solute mass to obtain the diffusion equation:

$$\frac{\partial C}{\partial t} = D_m \nabla^2 C. \quad (2.34)$$

Typically the values for the molecular diffusion coefficient are small and therefore diffusion only operates over short distances. For spherical particles with radius r the diffusion coefficient is given by the *Stokes-Einstein equation* ([Einstein, 1905](#)):

$$D_m = \frac{k_B \cdot T}{6\pi\mu r} \quad (2.35)$$

with the *Boltzman constant* k_B , absolute temperature T ($[T] = K$), and dynamic viscosity μ of the fluid.

2.6.2 Taylor-Aris Dispersion

Dispersion is a mixing mechanism of solute species due to differential flow in porous media or generally thin flow domains, where the influence of boundaries on the flow is strong. The flow is typically much slower near to the boundaries of the pores or to the walls, as given in Hele-Shaw cells (cf. equation (2.30)). In such flow geometries molecular diffusion as described above samples the flow in transverse direction. Particles of the solute diffuse randomly perpendicular to the direction of mean flow and therefore jump to regions of the flow with either higher or slower velocities. For long time scales compared to the process of molecular diffusion the individual solute particles diffuse several times across the entire diameter of the flow channel, representing the pores. In other words, the solution is well mixed in transverse flow direction with respect to the solute particles. Since the particles jump between regions of different flow velocity, any concentration distribution will spread in lateral flow direction, which is referred to as *Taylor-Aris dispersion*. This spreading for well mixed transverse concentrations acts similar to molecular diffusion, but is only apparent in moving fluids. The diffusion coefficient has to be adapted accordingly with an effective diffusion:

$$D_{eff} = D_m + \gamma \frac{\bar{v}^2 l^2}{D_m}, \quad (2.36)$$

where γ is a dimensionless parameter to account for the shape of the considered pore, l is the characteristic length, and \bar{v} is the averaged velocity in this pore ([Aris, 1956](#)). Note that this formulation only describes dispersion in single pores, i.e. it is only valid for the microscopic scale in porous media. However, it applies for Hele-Shaw cells as well as they consist of just one large pore. Therefore, the discussion of the transition to the macroscopic description is omitted here. For a derivation of the macroscopic description involving the approach of hydrodynamic dispersion see [Roth \(2012\)](#).

2.6.3 Convection Dispersion Equation

The previously introduced mechanisms of solute transport generally superposes with the fluid motion. By pure convection solutes are transported with the flow:

$$\frac{\partial C}{\partial t} = -\mathbf{v} \cdot \nabla C. \quad (2.37)$$

Combining convection (2.37) and diffusion (2.34) and accounting for dispersion yields:

$$\frac{\partial C}{\partial t} = -\mathbf{v} \cdot \nabla C + D_{eff} \nabla^2 C, \quad (2.38)$$

which is called the *convection dispersion equation* (CDE) or *convection diffusion equation* for negligible dispersive effects. Then the effective diffusion coefficient D_{eff} is replaced by the coefficient for molecular diffusion D_m . Note that generally the diffusion coefficient has to be described by a dispersion tensor \mathbf{D} for non-isotropic media.

With this relation the set of equations is closed to describe density-driven flows in Hele-Shaw cells.

2.7 Active Solute Transport

In this practical course processes regarding *active solute transport* is experimentally modeled, which essentially corresponds to the *Rayleigh-Taylor instability* (RTI) with respect to altering the density of water by the presence of a single solute.

Generally, RTI arises at the interface of two fluids with differing densities, when the less dense fluid is pushing the more dense one ([Sharp, 1984](#)). Small perturbations of the interface lead to growing instabilities in the form of fingers or plumes. Here, the fluids are either immiscible or miscible leading to different cases of RTI. For the immiscible RTI the destabilizing effect of the density stratification is counteracted by surface tension. In the miscible case the stabilizing effect is represented by diffusive transport at the interface.

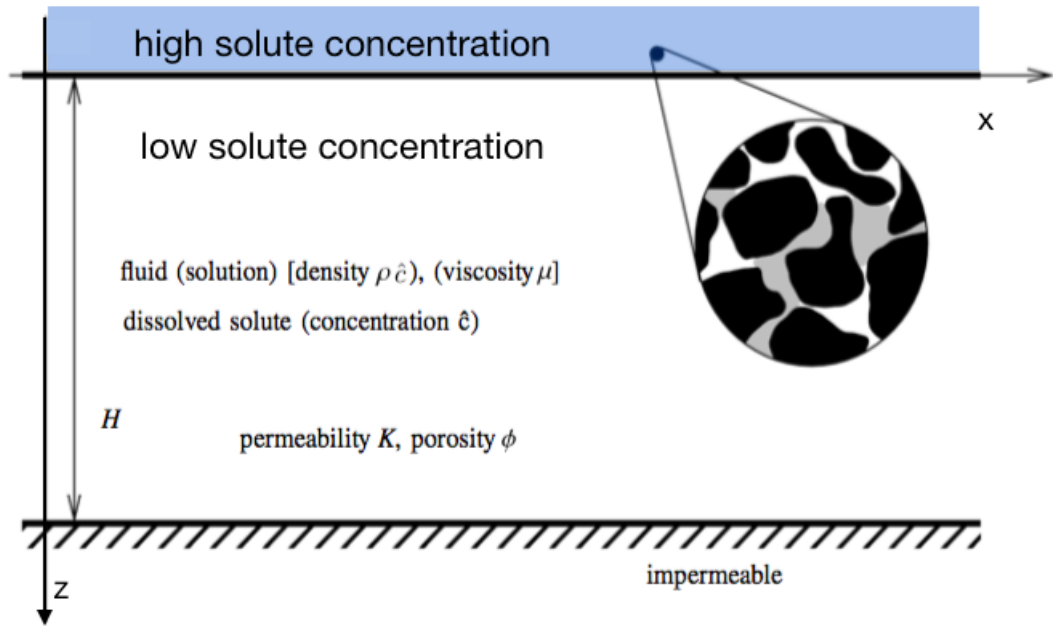


Figure 2.2: Schematic sketch of the initial situation that possibly leads to density-driven flow instabilities. Fluid with high solute concentration is placed above fluid with low solute concentration. Figure adopted from *Slim* (2014).

Depending on the relative magnitude of the stabilizing and destabilizing effects the formation of the fingers and the plumes develops or is prevented.

The situation investigated in the scope of this course resembles the latter case of miscible RTI, where a more dense solution with higher solute concentration initially rests on top of solution with lower solute concentration both subjected to Earth's gravitational field. Along with this the flow domain is given by the introduced geometry of Hele-Shaw cells leading to the modeling of the flow in a porous medium.

Side Note: Another interesting and similar instability to RTI is the Saffman-Taylor instability (*Saffman and Taylor, 1958*), where the instability is caused by differences in the viscosity of the fluids of interest, when the less viscous fluid is penetrating a domain containing a more viscous one. Given a close similarity the above mentioned problems are usually treated with equal concepts, as it is presented in the following for the miscible RTI considered in this course.

To describe the dynamics of the RTI in the miscible case in Hele-Shaw cells caused by concentration difference of a single solute we consider the initial situation depicted in Figure 2.2. The set of partial differential equations is then already given by the equations (2.28), (2.32), and (2.38). By coupling with the equation of state (2.20) these combine to

$$\nabla \mathbf{v} = 0, \quad (2.39)$$

$$\mathbf{v} = -\frac{k}{\mu} (\nabla p - \rho(C) \mathbf{g}), \quad (2.40)$$

$$\frac{\partial C}{\partial t} = -\mathbf{v} \cdot \nabla C + D_{\text{eff}} \nabla^2 C, \quad (2.41)$$

$$\rho(C) = \rho_0 + (\rho_1 - \rho_0) \cdot C \quad (2.42)$$

with the according boundary conditions of

$$\mathbf{v}_z = 0, \quad \frac{\partial C}{\partial z} = 0 \quad \text{at} \quad z = H \quad (2.43)$$

for an impermeable lower boundary and

$$C = C_{\text{max}} \quad \text{at} \quad z = 0 \quad (2.44)$$

for the upper boundary. Here the *continuity equation*, the *Darcy's law*, the *convection dispersion equation*, and the equation of state for water with respect to the solution of a single solute are already given for the special case of Hele-Shaw flow of incompressible fluid, meaning that the porosity is set to $\phi = 1$ and the density ρ is solely altered by the addition of the solute. As the flow occurs in a two dimensional domain, $\rho(C(x, z, t))$ and $p(x, z, t)$ represent the density and pressure fields. The gap averaged velocity is given by $\mathbf{v} = (u, w)$ and the gradient has two components only defined in these two directions: $\nabla = (\partial_x, \partial_z)$.

2.7.1 Dimensionless Formulation

As for other systems in fluid dynamics it is conventional to render the governing equations dimensionless by choosing characteristic quantities. In the following a characteristic velocity U_c and length scale L is introduced.

The characteristic velocity is represented by the buoyancy velocity:

$$U_c = \frac{\Delta \rho \cdot g \cdot k}{\mu}, \quad (2.45)$$

which is the falling velocity of a fluid parcel with maximum solute concentration in the porous medium. The adequate length scale is the diffusion length:

$$L = \frac{\phi D_m}{U_c} \quad (2.46)$$

over which diffusion and convection balance each other. The characteristic density is chosen as the difference between the maximal and minimal density ρ_1 and ρ_0 :

$$\varrho_c = \Delta \rho = \rho_1 - \rho_0. \quad (2.47)$$

Marking with a hat, we set the dimensionless quantities to

$$\hat{\mathbf{v}} = \frac{\mathbf{v}}{U_c}, \quad \hat{\mathbf{x}} = \frac{\mathbf{x}}{L}, \quad \hat{\rho} = \frac{\rho}{\rho_c} \quad \text{and} \quad \hat{t} = \frac{U_c}{\phi L} t \quad (2.48)$$

and the derivatives to

$$\frac{\partial}{\partial \hat{t}} = \frac{\phi L}{U_c} \frac{\partial}{\partial t} \quad \text{and} \quad \hat{\nabla} = L \nabla. \quad (2.49)$$

The dimensionless equations then take the form:

$$\hat{\nabla} \hat{\mathbf{v}} = 0, \quad (2.50)$$

$$\begin{aligned} \hat{\mathbf{v}} &= - \left(\frac{k}{\phi \mu D_{eff}} \hat{\nabla} (p - \rho_0 g z) - c \cdot \mathbf{e}_z \right) \\ &= - \left(\hat{\nabla} \hat{p} - c \cdot \mathbf{e}_z \right), \end{aligned} \quad (2.51)$$

$$\frac{\partial c}{\partial \hat{t}} = - \hat{\mathbf{v}} \cdot \hat{\nabla} c + \hat{\nabla}^2 c, \quad (2.52)$$

$$\hat{\rho} = \hat{\rho}_0 + c. \quad (2.53)$$

Here, for the pressure $\hat{p} = k/(\mu L U_c)(p - \rho_0 g z)$ has been introduced and c is again the reduced concentration as defined in equation (2.21).

From that dimensionless formulation the interesting findings become apparent at the domain boundaries. For the upper boundary the dimensionless formulation yields

$$c = 1 \quad \text{at} \quad \hat{z} = 0 \quad (2.54)$$

and for the lower boundary

$$\hat{\mathbf{v}}_z = 0, \quad \frac{\partial c}{\partial \hat{z}} = 0 \quad \text{at} \quad \hat{z} = \frac{\Delta \rho g k H}{\mu \phi D_{eff}} = \text{Ra}, \quad (2.55)$$

where H is the height of the flow domain. There are two remarkable conclusions coming from this dimensionless formulation. First, the governing equations are rendered completely parameter free, which means that the evolution of the system, if observed in the dimensionless framework is universal. Second, the only parameter, the *Rayleigh number* Ra, just occurs at the position of the lower boundary. To understand this conclusions in more detail we take a look at the evolution of the system first before we discuss the meaning of Ra.

2.7.2 Density-Driven Convection Regimes

First we want to assume a flow domain with a very large depth H and therefore large value of Ra. In this case the evolution of the system is determined by the initial situation at the upper boundary and how the solute is transported into deeper layers. The presence of the lower boundary does not interfere with this evolution until very long times. The classification of the individual regimes is adopted from [Slim \(2014\)](#).

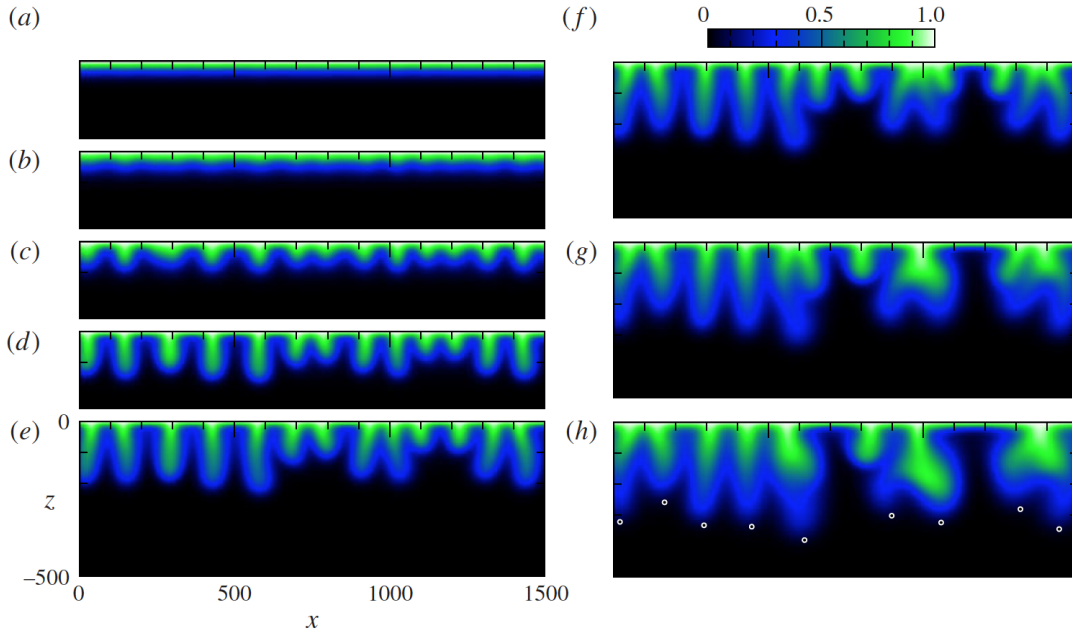


Figure 2.3: Numerical simulation results for the concentration fields of the density-driven instability depicting the onset. Figure adopted from *Slim* (2014).

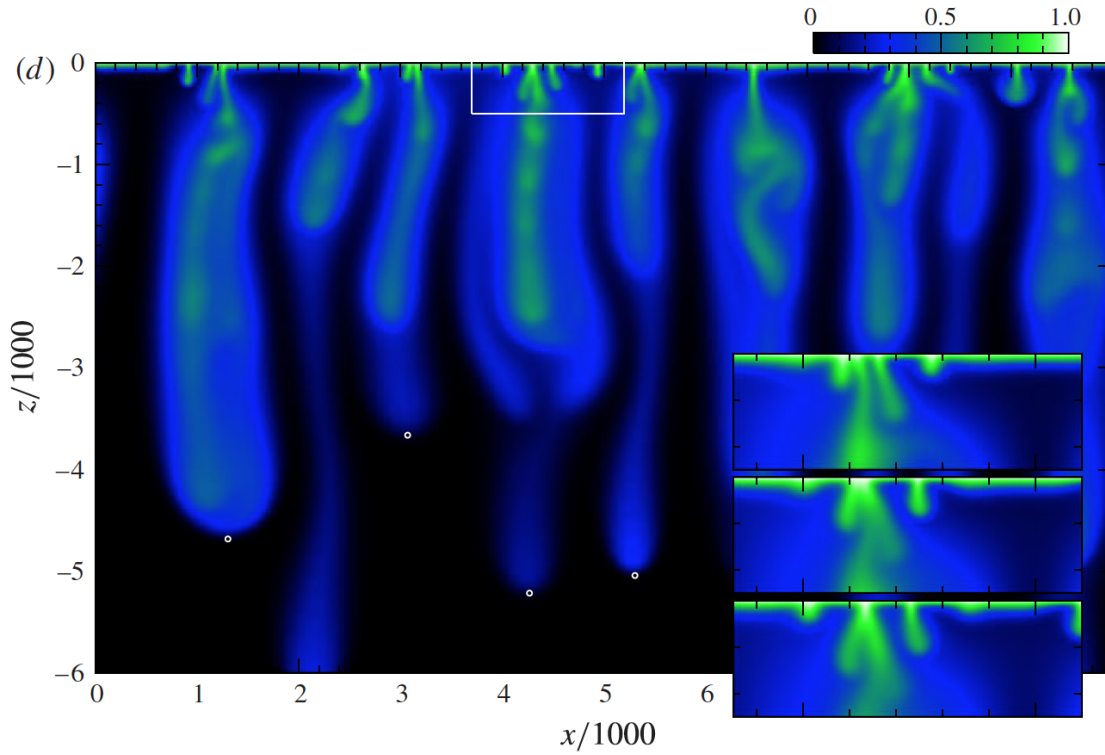


Figure 2.4: Numerical simulation results for the concentration fields of the density-driven instability depicting later time steps. Figure adopted from *Slim* (2014).

The diffusive regime. At first the transport of the solute at the upper boundary is purely accounted by diffusion as it is sufficiently fast for short distances. Also the diffusion and buoyancy driven convection compete each other as it is illustrated in Figure 2.5. Diffusion smoothes out initial perturbations in the density gradient before convection sets in. A depiction of the according concentration field is given in Figure 2.3 (a).

The linear-growth regime. In the second regime enough dense material has accumulated beneath $z = 0$ for the convection to overcome diffusion. At this stage faint perturbations become distinguishable from the purely diffusive density profile that has evolved up to this point (see Figure 2.3 (b)). This is due to their amplification by convection, however the perturbations are barely noticeable and the transport is still governed by diffusion.

The flux-growth regime. Now the faint perturbations have grown to form macroscopic convection fingers, as depicted in Figure 2.3 (c) through (e), that begin to influence the mass transport. This is because they strip dense material that has accumulated due to diffusive transport beneath the boundary layer. As the dense material is transported away from the boundary the dissolution flux of solute there is enhanced and therefore marks the regime of flux-growth. Throughout the flux-growth the fingers strengthen and elongate with a key characteristic that the lateral motion is very limited. This results in fixed positions of the finger roots. While these first macroscopic fingers are regularly spaced, some pioneer the others slightly, depending on the initial perturbations that occurred during the linear-growth regime.

The merging regime. During the fourth regime the fingers begin to merge (cf. Figure 2.3 (f) through (h)). As the pioneering fingers outgrow the slower ones, they begin to generate velocity field that strongly influences their environment and the fingers enter non-linear interaction with another. At positions where fingers are lagging behind they can be forced to retreat due to the upwelling return flow caused by their neighbors. In regions where fingers are comparably long and slightly closer together they get pushed towards each other by the upwelling flow exterior to them until they zip together beginning from the root downward. Mainly these processes lead to a coarser spacing of the fingers, when compared to the flux-growth regime. Possibly more than one generation of this coarsening can occur during this stage until the dominant fingers have established and govern their whole environment with larger spaces in between, where low-solute fluid rises up.

The constant-flux regime. Because of the previous merging of the fingers, the spacing between the resulting dominant fingers is sufficiently wide to become unstable by the same process as at the beginning of the temporal development. Therefore, new fingers reinitiate in the regions between the dominant fingers and are swept into them by the governing flow field. This can be seen in the inset of Figure 2.4. The reinitiation can be interpreted as the marginal stability of the diffusive layer (*Howard, 1964*), (*Doering and*

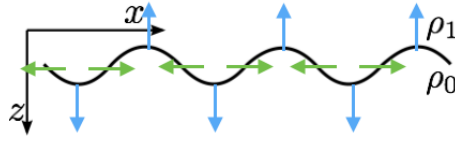


Figure 2.5: Schematic of the competing processes at initial small disturbances. Buoyancy induced convection (blue arrows) amplify the existing disturbances due to the density contrasts ($\rho_1 > \rho_0$), whereas diffusion (green arrows) smears out the density contrasts and therefore counteracts the convection.

(Constantin, 1998) between the dominant fingers as the layer thickens by diffusion, if it is too thin, but single fingers develop as the layer gets too thick. This process balances the transport process and leads to a constant flux of solute into the flow domain.

The shut-down regime. This regime is the last and terminates the temporal development of the system. Independent of the current regime the shut-down starts, when the solute reaches the lower boundary of the flow domain either by diffusion or convection. From this point on the domain starts to saturate with the solute and all the phenomena, as merging, reinitiation, and diffusion are slowing down due to the more and more decreasing density gradients.

2.7.3 Meaning of the Rayleigh Number

To explain the Ra parameter two interpretations of the parameter are given. First a more common one, as it is more intuitive and also describes some important aspects and second a more refined interpretation, as the common interpretation lacks, as we think, some important aspects to understand the development of the density-driven instabilities. Commonly the *Rayleigh number* is thought of as the ratio between the flow induced by buoyancy to the speed of diffusion across the layer, as it is indicated by the definition

$$Ra = \frac{\Delta \rho g k H}{\mu \phi D_{eff}} = \frac{U_c H}{\phi D_{eff}} \hat{=} \frac{\text{buoyancy}}{\text{diffusion}}. \quad (2.56)$$

From this it becomes quite clear that Ra is a measure for the magnitude of the instability, where a higher value of Ra means a more unstable situation, as buoyancy is the driving aspect due to vertical density gradients (equation (2.45)) that are smeared out by diffusion (equation (2.33)). This competition of the processes is also illustrated in Figure 2.5. Whereas the above are meaningful statements about the system behavior, this particular concept exposes its flaws, when we direct the attention to the layer height H in the formulation. The assumption that the situation becomes more unstable with increasing layer height H is obviously wrong, since the stability can only be determined by the system parameters ($\rho(c)$, μ , k , ...) directly at the upper boundary. Therefore, we shift the perspective on Ra and interpret it as the dimensionless depth of the flow domain

as it is apparent in equation (2.55).

In this second interpretation, it is important to understand that the process we are looking at is a transient one. The temporal development is described by the dimensionless formulation given by equations (2.50), (2.51), (2.52), and (2.53), which is completely parameter free revealing its universality. This means such systems always develop instabilities and encounter all the temporal regimes, if the lower boundary is sufficiently far away. If the lower boundary is sufficiently far away, is determined by the Ra parameter that scales the actual depth of the flow domain accordingly to the initial conditions. This dimensionless depth then interferes with the temporal development of the system, when the presence of the lower boundary is encountered by the transport process.

2.7.4 Critical Values

The investigation of the marginal stability of the system is frequently addressed by linear stability analysis, as for example done by *Riaz et al. (2006)* and *Fernandez et al. (2001)*. Linear stability analysis gives insight into the conditions under which the instabilities occur and delivers values for critical measures. Especially interesting for this course are the values of the critical time t_{crit} and the critical wavelength λ_{crit} . For this course we want to skip the details of the linear stability analysis and focus on the results of *Riaz et al. (2006)*.

Riaz et al. (2006) theoretically and numerically regard the problem of CO₂ sequestration in deep geological formations. Therefore they investigate the stability of a fluid with a dissolved substance altering the density at the upper boundary of the flow domain in a porous medium. The solute in this case is introduced by solution of CO₂ right at the interface between the water and the gas phase. Their choice for the characteristic length scale is the height of the domain H . As their findings rely on an analogue system to the experiments conducted in this course, the results are taken as theoretical predictions.

From their considerations, they deduce:

$$t_{\text{crit}} = a \frac{\phi \mu^2 D_m}{(k \Delta \rho g)^2} \quad (2.57)$$

and

$$\lambda_{\text{crit}} = \frac{2\pi \mu D_m}{bk \Delta \rho g}, \quad (2.58)$$

with the parameters $a = 146$ and $b = 0.07$.

Since these values, as the various values given in the literature, are derived by theoretical and numerical analysis only, one aim of this course is to make an experimental approach on these values and record several data points for different initial conditions over time.

3 Experimental Setup, Methods, and Equipment

Preliminarily you should note that some of the equipment described below is **delicate and expensive laboratory equipment**. Therefore you are requested to **handle all the instruments with care and ask the tutor, if anything about the equipment is unclear**.

3.1 Experimental Setup

A schematic of the experimental setup is shown in figure (3.1). The setup is used to observe the fluid flow in our flow domain, the Hele-Shaw cell, using a light transmission method by exploiting the absorption by an appropriate dye. The light transmission method is explained in detail in section 3.2.

The Hele-Shaw cell consists mainly of two parallel glass plates of dimensions 30 cm x 50 cm, which are held together by an aluminum frame as depicted in figure (3.2). The glass plates are separated by either a silicone seal alone or by a combination of a PVC frame (not depicted in the figures) and silicone seal. The resulting gap width is then either left empty or filled with small glass beads to serve as the flow domain for the experiments. In several cases canulas are used as inlets along the sides of the Hele-Shaw cells to enable the filling of the Hele-Shaw cell from below and attach, as depicted exemplarily in figure (3.1), several fluid reservoirs.

Behind the Hele-Shaw cell, there is a light source consisting of a LED-array with an optical diffusor up front, which is made from a translucent acrylic glass plate. This components are used to provide a relatively uniform light intensity over the whole Hele-Shaw cell. Here, three different kinds of high intensity LEDs are used, which emit at the main wavelengths of 450 nm, 505 nm, and 625 nm. Due to the blue light components of the emitted spectrum **do not stare into the LED light source to avoid harm to the retinal tissue of your eyes**.

The intensity of the light transmitted through the Hele-Shaw cell is observed by a CCD-camera (*AVT Pike F505B*), which is equipped with an optical filter wheel to enable the observation at different wavelengths. The provided optical filters are narrow band pass filters, which are matched to the wavelengths of the used LEDs in the light source (452 ± 9 nm, 502 ± 10 nm and 632 ± 11 nm). Therefore an appropriate overlap of the emission spectra of the LEDs and the observation windows of the filters is given.

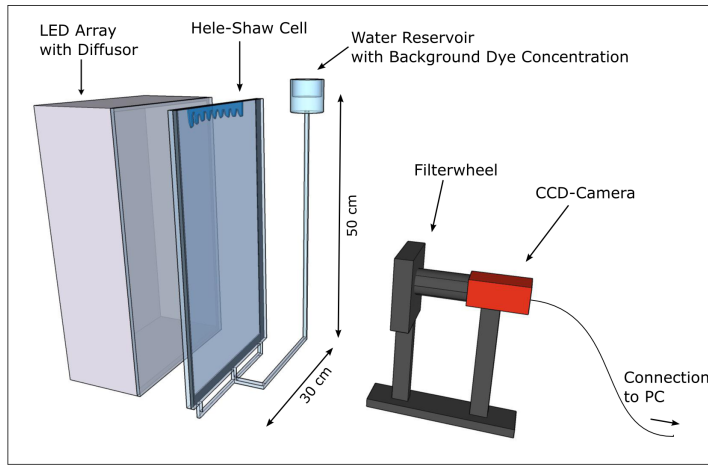


Figure 3.1: Illustration of the experimental setup. Depicted are the main components: Hele-Shaw cell, LED-array with diffusor, the CCD-camera with the attached filterwheel, and in this case a fluid reservoir that is attached to the bottom of the Hele-Shaw cell. Figure from [Kreyenberg \(2015\)](#).

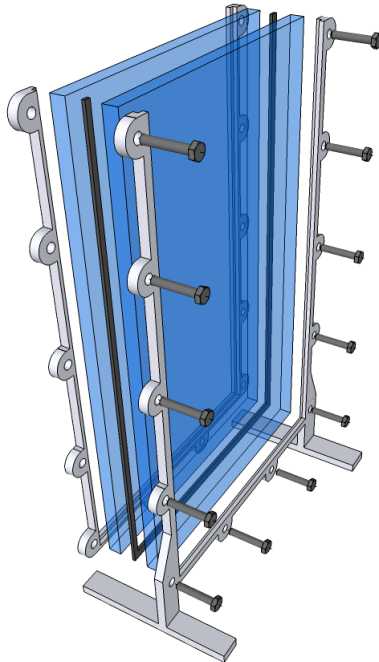


Figure 3.2: Exploded view of the Hele-Shaw cell showing the parallel glass plates, sealant material and the aluminum frame.

3.2 Measurement Method

The light transmission measurement method used for the experiments is based on the *Lambert Beers law* and the absorption of the light by a dye added to the water to the water in the Hele-Shaw cell. Assuming the one dimensional case of the Hele-Shaw cell with respect to the light path, the extinction for monochromatic light at wavelength λ for a water-dye solution filled gap is given by:

$$\epsilon_{\lambda}(C_{\text{dye}}, d) = \epsilon_{\text{instrument}} + \alpha_{w,\lambda} \cdot d + \alpha_{\text{dye},\lambda} \cdot C_{\text{dye}} \cdot d = -\log \left(\frac{I_{\text{out},\lambda}(C_{\text{dye}}, d)}{I_{\text{in},\lambda}} \right), \quad (3.1)$$

with the extinction $\epsilon_{\text{instrument}}$ given by the parts of the experimental setup (e.g. glass plates...), the absorption coefficient $\alpha_{w,\lambda}$ of the water in the gap with width d , the absorption coefficient $\alpha_{\text{dye},\lambda}$ given by the addition of the dye with concentration C_{dye} , the intensity of the incident light $I_{\text{in},\lambda}$, and the attenuated light intensity $I_{\text{out},\lambda}$. When measuring the intensities at different dye concentrations $C_{\text{dye},1}$ and $C_{\text{dye},2}$ with $C_{\text{dye},2} > C_{\text{dye},1}$ we can calculate the difference in the extinction:

$$\Delta\epsilon_{\lambda}(C_{\text{dye},1}, C_{\text{dye},2}, d) = \alpha_{\text{dye},\lambda} \cdot d \cdot (C_{\text{dye},2} - C_{\text{dye},1}) = -\log \left(\frac{I_{\text{out},\lambda}(C_{\text{dye},2})}{I_{\text{out},\lambda}(C_{\text{dye},1})} \right). \quad (3.2)$$

Applying these findings to the two dimensional observations of the CCD-camera, which records gray values $g(x, y)$ ideally being proportional to the light intensities at the individual pixels $g(x, y) \propto I(x, y)$ we conclude:

$$-\log \left(\frac{I_{\text{out},\lambda}(C_{\text{dye},2}, x, y)}{I_{\text{out},\lambda}(C_{\text{dye},1}, x, y)} \right) = -\log \left(\frac{g(C_{\text{dye},2}, x, y)}{g(C_{\text{dye},1}, x, y)} \right) = \alpha_{\text{dye},\lambda} \cdot d(x, y) \cdot (C_{\text{dye},2}(x, y) - C_{\text{dye},1}(x, y)) \quad (3.3)$$

Supposed the absorption coefficient $\alpha_{\text{dye},\lambda}$ is known either of the unknowns $d(x, y)$, $C_{\text{dye},1}$ and $C_{\text{dye},2}$ can be determined by measuring the remaining two. This is used in the experiments to determine the gap width $d(x, y)$ by taking calibration measurements with known homogeneous dye concentrations within the Hele-Shaw cell or to observe the concentration fields over time due to the density driven instabilities.

3.3 Explanation of the Equipment

Additionally to the core of the experimental setup several other instruments are used to determine parameters or to provide different boundary conditions for the experiments. In this section these peripherals are presented and their usage is explained.

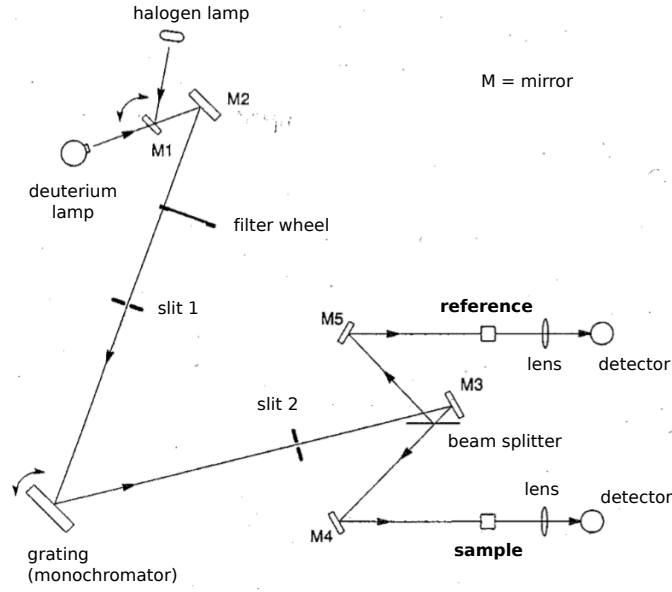


Figure 3.3: Schematic view of the spectrometers optical system.

3.3.1 Camera

The current camera to perform calibration measurements and record the images during the experiments is an AVT Pike F-505b with a CCD-sensor. The important properties of the camera are the linearity of the sensor, meaning that a linear increase of the incoming light intensity leads to a linear response of the pixels wrt the output gray values, and the signal to noise ratio.

The assumption for the linear response in gray value g of the camera to the number of photons N can be described by:

$$g = g_{\text{dark}} + \alpha N, \quad (3.4)$$

where g_{dark} is the dark current and α the factor of proportionality. Since the interest during the measurements is on the relations between the number of photons N , we only need to correct for the dark current, as α is a property of the camera and constant for all measurements. **Note that the assumption of linearity only holds until 80% of the saturation value for the camera chip.**

The camera returns values in 14 Bit depth, which means it returns values in the range of $[0, 65530]$.

The object lens of the camera provides the manual setting of the aperture to adapt brightness of the images and the manual setting of the focal point.

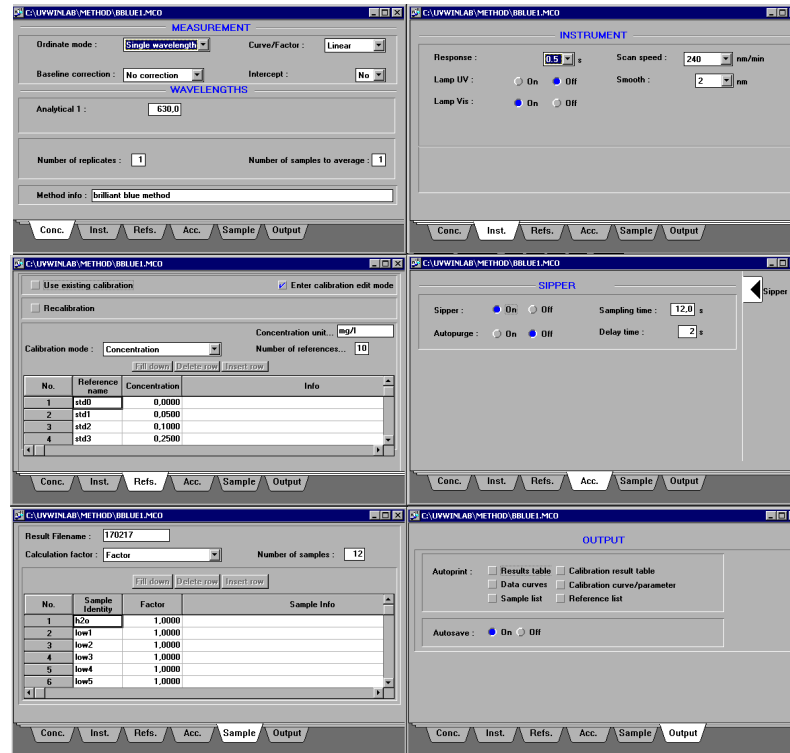


Figure 3.4: Depiction of the parameter setup for the spectrometer measurement.

3.3.2 Spectrometer

To obtain reference measurements for the concentrations of the tracer an optical spectrometer is used. The schematic of the light path is shown in Figure 3.3. In general the spectrometer implements the same measurement principle based on *Lambert Beers law* as described in section 3.2, with the difference that the length of the light path through the tracer solution is fixed and known. Therefore, with the according calibration through standard solutions, the measured values of the light extinction can be related to the sample concentration.

The setup allows for different measurement types. Either the extinction of light at a distinct wavelength according to the analyzed tracer concentrations (cf. Figure 3.6) can be measured or the whole absorption spectrum of a tracer can be investigated (cf. Figure 3.5), with the main purpose for this practical course being the concentration determination of tracer samples needed to calibrate the measurements using the Hele-Shaw cell. For this it is important to note that the observable concentration range of the spectrometer is much smaller than the tracer concentrations used in the experiments. Therefore the samples have to be diluted accordingly to be able to investigate them with the spectrometer. The measurement range of the spectrometer for Brilliant Blue in this case is $C_{BB} = 0 \dots 25 \text{ mg/l}$, before the tracer solution gets practically opaque for the spectrometer and results in a saturated light extinction value.

The standard procedure to determine the concentration of a tracer sample is:

1. By using pipettes and volumetric flasks dilute your tracer sample with de-ionized

- water to match the measurements range of the spectrometer.
2. Turn on spectrometer.
 3. Boot measurement computer and enter password (password on monitor)
 4. Open the program UVWINLAB PHOTOMETER on the desktop and enlarge the window to full screen by clicking the square button in the upper right corner. Check the status of the spectrometer which is displayed at the bottom of the now enlarged window. The status should be Instrument ready before you proceed.
 5. At the spectrometer, clamp the tube into the pumping mechanism without turning the screw and make sure the long end of the tube is inside the waste bottle.
 6. Put a beaker with de-ionized water under the sipper and suck the de-ionized water into the tube by pressing the right arrow key until the tube is filled up to the waste bottle. If air is sucked into the tube while the pump is in resting position, really carefully tighten the screw at the pumping mechanism until no air is sucked in anymore.
 7. In the control program open the tab Conc in the Methods window and choose BBLUE1.MCO by double clicking.
 8. Set up all the parameters. Default parameters are given in Figure 3.4. The only tab that needs the adaption to your measurement is the Sample tab. There enter a filename for your measurement and enter the number of samples you want to analyze starting and ending with a sample of de-ionized water. To get a better estimation of the error for your concentration it is necessary to measure a single sample multiple times, so take that into account for the number of samples.
 9. Click on Start at the upper left to start recording the calibration curve with the standard concentration samples.
 10. In the lower left corner, the program prompts for the sample to analyze next. It starts to ask for a blank sample of de-ionized water and then continues with the standard concentration samples. To measure the samples place the sample under the sipper and press the larger black key behind the sipper.
 11. Take the standard concentration samples and once turn the flask upside down to ensure that condensed water beneath the cap is mixed with the solution. Measure the standard concentration samples in increasing order.
 12. When finished, check the correlation coefficient to be nearly 1 and answer the prompt of the program by clicking ok. If the fitted curve fits to the data you can proceed to analyze the sample by clicking Analyze samples. The program will then prompt for the according samples.
 13. When finished with the measurement of all the samples, purge the instrument by

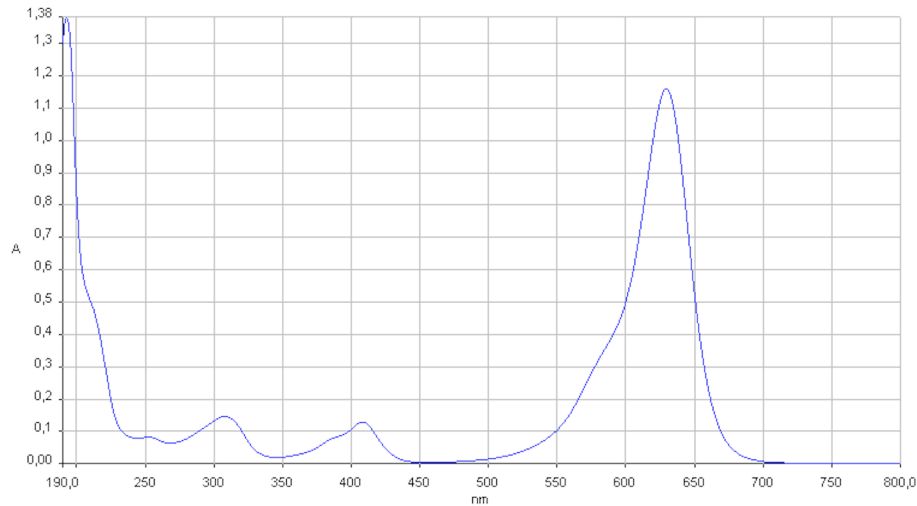


Figure 3.5: Absorption spectrum of Brilliant Blue at $C = 10\text{mg/l}$.

pumping a good amount of de-ionized water by pressing the right arrow key at the sipper of the spectrometer. Then loosen the pumping mechanism and loosen the tube.

14. When closing the control program it should automatically prompt you to save the data.
15. In the file explorer navigate to the output directory `c:_UVWINLAB_DATA` and transfer the corresponding RCO file to a USB pen drive.
16. Turn off the computer and the spectrometer.

3.3.3 Brilliant Blue

The dye used in this practical course is the food grade dye *Brilliant Blue* (BB) and acts as a tracer to be able to make observations of the flow phenomena. Since it is a food grade dye, it does not introduce any health risk at normal concentrations, however it is a chemical substance that, in high concentrations, **causes serious eye irritation, may cause skin irritation, and causes damage to organs through prolonged or repeated exposure**. Also BB is **very capable of staining** things blue (your fingers, clothes, etc.) so be **very cautious when handling higher concentrations** and **always wear safety glasses and lab coats!**

This section introduces the properties of BB needed to conclude results from the measurements.

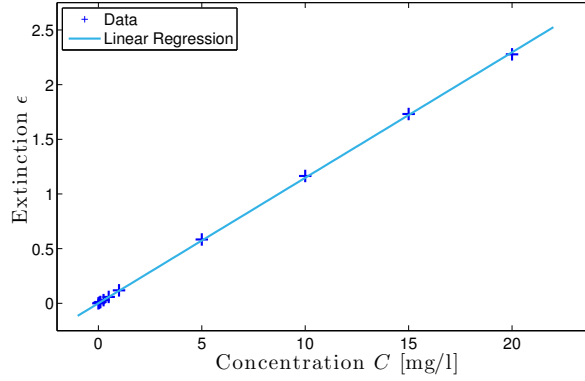


Figure 3.6: Extinction of light measured at ten distinct Brilliant Blue concentrations to determine the absorption coefficient α_{BB} at wavelength $\lambda = 630\text{nm}$. Figure from [Kreyenberg \(2015\)](#).

Absorption Coefficient

To make any conclusions from the light intensity measurements with the experimental setup described above, the absorption coefficient of BB has to be determined. This is done with the spectrometer (cf. section 3.3.2) where also the *Lambert Beers law* (3.1) for the zero calibration of a water filled cuvette in the form:

$$\epsilon_{\lambda}(C_{\text{BB}}) = -\log\left(\frac{I_{\lambda}(C_{\text{BB}})}{I_{0,\lambda}}\right) = \alpha_{\text{BB},\lambda} \cdot C_{\text{BB}} \cdot d, \quad (3.5)$$

where the light intensity $I_{\lambda}(C_{\text{BB}})$ is the transmitted fraction of the initial intensity $I_{0,\lambda}$ over the light path d with containing a solution with the concentration C_{BB} . The light path $d = 10\text{mm}$ is the fixed thickness of the cuvette installed in the spectrometer.

Exemplarily, the determination results of $\alpha_{\text{BB},630\text{nm}}$ at the absorption maximum of BB at $\lambda = 630\text{nm}$ (cf. Figure 3.5) is shown. Figure 3.6 presents the measurements for ten BB standard solutions in the range $C_{\text{BB}} = 0 \dots 20\text{mg/l}$. From the linear regression, the absorption coefficient is determined to be $\alpha_{\text{BB},630\text{nm}} = (1.148 \pm 0.004) \times 10^4 \text{m}^2/\text{kg}$ by solving (3.5) with respect to $\alpha_{\text{BB},\lambda}$.

Diffusion Coefficient

To be able to make any predictions about the Rayleigh number it is necessary to know the molecular diffusion coefficient $D_{\text{m,BB}}$ of the tracer. In the case of Brilliant Blue this is a bit problematic, since there is no data available by the manufacturer and the diffusion coefficient is not easily available to measurements. Therefore a rather crude assumption is applied here. For this the *Stokes Einstein equation* (2.35) is applied, which relates the drag on spherical particles due to Brownian motion to the molecular diffusion coefficient. Considering the chemical structure of the Brilliant Blue molecule (cf. Figure 3.7) and estimating the spatial extent with the appropriate bond lengths leads to an approximation of the radius $R_0 \sim 7.5 \pm 2.5\text{\AA}$. This results in a diffusion coefficient of

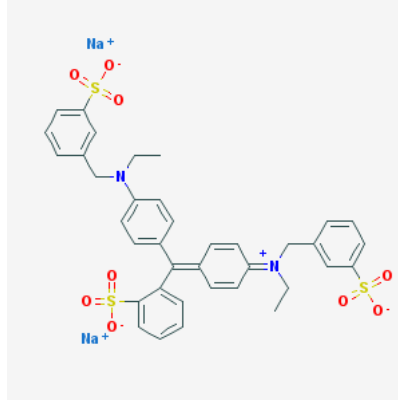


Figure 3.7: Chemical structure of Brilliant Blue (*National Center for Biotechnology Information*, 2015).

$D_{m, BB} \sim (2.9 \pm 1.0) \times 10^{-10} \text{ m}^2/\text{s}$ at room temperature. Again, note that this is a rough estimation, since the molecule is not spherical and has nine rotatable bonds, which enables several geometric configurations.

Solutal Expansion Coefficient

Another important property to conclude relations between the observed concentrations and the density differences during the experiments is given by the solutal expansion coefficient of Brilliant Blue β_{BB} . Here a method to estimate that property is shortly introduced. With a Gay Lussac type pycnometer and a high precision balance the density has been determined several times for three distinct concentration samples of Brilliant Blue solution. The results are illustrated in Figure 3.8 with the solutal expansion coefficient being derived from the linear regression. This leads to $\beta_{BB} = (1.90 \pm 0.15) \times 10^{-4} (\text{kg l})/(\text{mg m}^3)$. Note that the data points with three concentration samples is relatively sparse and therefore the assumption of a linear relation might be wrong.

Summary

Property	Value	Dimension
Absorption coefficient $\alpha_{BB, 630m}$	1.148 ± 0.004	$10^4 \text{ m}^2/\text{kg}$
Diffusion coefficient $D_{m, BB}$	2.9 ± 1.0	$10^{-10} \text{ m}^2/\text{s}$
Solutal expansion coefficient β_{BB}	1.90 ± 0.15	$10^{-4} (\text{kg l})/(\text{mg m}^3)$

Table 3.1: Summary of the important properties of Brilliant Blue. Table from *Kreyenberg* (2015).

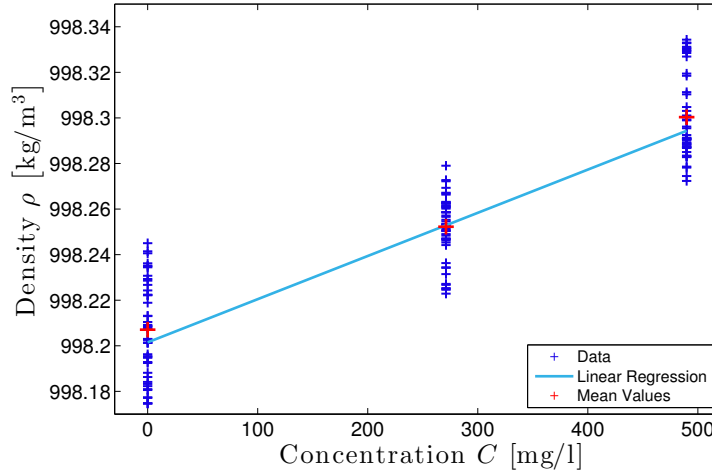


Figure 3.8: Determination of the density of three Brilliant Blue concentration samples to derive the solutal expansion coefficient β_{BB} by linear regression. Figure from [Kreyenberg \(2015\)](#).

3.4 Explanation of the Scripts

To evaluate the recorded image series and to control the CCD-camera some software and scripts are provided. How to use this software and set up the measurements is introduced in the following.

3.4.1 Image Acquisition

To control the CCD-camera, the filterwheel, and the light source for the image acquisition the Matlab script collection `AVT_Pike_camera_ctrl` is used, which is available on the laboratory computer. In this section the usage is explained and the important features are introduced.

How to run the script. To start Matlab open a Terminal and navigate to the directory containing the scripts with `cd /home/f59/lm_ctrl` or go there with the file explorer and open a Terminal by clicking right and choosing the corresponding option. In the terminal type `./start_matlab.sh` and press enter, which will start Matlab with the needed settings. Then in the Matlab Command Window the script that controls the CCD-camera can be started by typing `image_acquisition('NAME_OF_INI_FILE.ini')`, where the desired settings are chosen in the respective INI-file. For these configurations two files are provided as templates: `adjust.ini` and `image_acquisition.ini`, which need to be edited first to fit the tasks of calibration and measurement. Depending on the directory you are in Matlab, an output folder is generated that contains the acquired images. By pressing `ctrl+c` the script can be stopped before it has finished.

How to set up INI-files. To set up the INI-files open the respective file with a text

editor and adjust it or copy one of the template files to create separate file and open this with a text editor. In the following the options to set up the image acquisition are discussed. The whole INI-file is divided in smaller blocks and the description of the options is given above the respective blocks.

In the general settings section the most important option is the specification of the output subdirectory to write the images of different measurements to different locations. The settings for the redirection should be set to 1 to write the output in the Command Window to a log file.

```
[general settings]
;subdirectory in directory ./output (e.g.: 'exp_2016-09-09')
output_directory_sub = adjust ;string
;redirection of stdout ot to 'stdout_log'. Possible values are 1/0 for yes/no
redirection = 1 ;bool
;logfile for standard output if redirection = 1
stdout_log = stdout.log ;string
```

Since the time stamps for the individual images received from the camera do not change between summer and winter time a workaround is introduced to correct for that.

```
[local time settings]
; There is a known problem with the image timestamps generated by the AVT Pike
  camera. The camera prints the time in UTC + 2 hours, which matches with
  the CEST in summer but not with CET in winter. To avoid inconsistencies in
  the log files, and given that "filename_style = unixtime", you can specify
  the current local time to correct for that: "CET" or "CEST"
local_time = CET
```

Four cooling fans are integrated into the light source that need to be switched on if the light source is switched on for a long period of time. The number of the power socket has to be set according to used power socket of the programmable surge protector.

```
[cooling fans settings]
;cooling fans mode: "on" or "off"
cooling_fans_mode = on
;power socket number on programmable surge protector
power_socket_fans = 3
```

The light source can be used in the continuous or alternating mode with the light source being switched on entirely or switched on before the acquisition of individual images and switched off afterwards. When the alternating mode is used a warm-up time needs to be specified. Also for the light source the number of the used power socket needs to be set.

```
[light source settings]
;light source mode: "continuous" or "alternating"
light_src_mode = alternating
```

```
;power socket number on programmable surge protector
power_socket_light_src = 4
;warmup time of the light source before images are taken [s]
light_src_warmup = 5 ;NOTE: When in alternating mode this adds up to
    'delay_sequence'
;name of log file
light_src_logfile = light_src.log ;string
```

When the experiments require volume monitoring of external fluid reservoirs, they can be placed on balances, which can be read out in the specified time steps. For this the ports of the balances need to be specified to match the setup (possible values are `/dev/ttyUSB0...`/`/dev/ttyUSB4`).

```
[balances settings]
;balances readout: "on" or "off"
balances_readout = off
;port the balance #01 is connected to
balance1_port = /dev/ttyUSB0 ;string
;port the balance #02 is connected to
balance2_port = /dev/ttyUSB1 ;string
;time interval of the balance readout [s]
balances_readout_interval = 1
; logfile for the balance readout
balances_logfile = balances.log ;string
```

In this section of the INI-file the actual options for the image acquisition are set. First the settings for the filterwheel are specified to match the current setup. There the port has to be specified (again with the possible values being `/dev/ttyUSB0...`/`/dev/ttyUSB4`) and the position at which the optical bandpass filters are installed have to be declared. If the value is set to 0 these filters will be skipped during the image acquisition. For the specified filters the script will loop over them and acquire the images at each position according to the additional settings. For the example below this means that images will be taken only for the 630nm filter, which is installed at position 2, and the dark current cover, which is installed at position 1. The delay defines a time interval, which will pass between the start of the script and the acquisition of the first image of the image series.

```
[image acquisition]
;port the filterwheel is connected to
filterwheel_port = /dev/ttyUSB2 ;string
;free filter position
pos_free = 0 ;int 5
;filter position of the 450 nm filter
pos_450 = 0 ;int 4
;filter position of the 500 nm filter
pos_500 = 0 ;int 3
;filter position of the 630 nm filter
pos_630 = 2 ;int 2
;filter position of the cover
```

```
pos_dark = 1 ;int 1
; how much delay shall this timer have?? [s]
delay = 2
;number of captured frames per shot (maybe used for averaging in future)
frames_per_shot = 1 ;int
```

Next, the camera gain for the individual filters can be specified, which is recommended to set to 0 and rather improve the brightness of the recorded images with the aperture settings at the objective.

```
;camera gain on no filter position
gain_free = 0;
;camera gain on 450 nm position
gain_450 = 0;
;camera gain on 500 nm position
gain_500 = 0;
;camera gain on 630 nm position
gain_630 = 0;
;camera gain on dark current position
gain_dark = 0;
```

To adapt the brightness values in the acquired images the exposure time has to be set accordingly. This is done for every filter by passing an integer value between 1 and 4095.

```
;exposure time: the exposure time is set with the exposure value ranging
;between 1 and 4095. The exposure times is the given by:
;exposure value x 20 s + 26 s.
;exposure time no filter
exposure_free = 1000 ;int
;exposure time 450 nm filter
exposure_450 = 4095 ;int
;exposure time 500 nm filter
exposure_500 = 2600 ;int
;exposure time 630 nm filter
exposure_630 = 1850 ;int
;exposure time with cover disk
exposure_dark = 1850 ;int
```

Besides the main loop in the script, which loops over the filter positions, an additional iteration number on each filter position can be given with `num_of_shots_filtername` to enable the acquisition of images at one filter position without the activation of the filterwheel. The delay specifies the time passing between two subsequent images at one filter position. After the script iterated over all specified filter positions it will wait for the time given by `delay_sequence` before it returns to the first filter. The number of iterations over all filter positions is specified by `cycles`.

```
;number of shots taken without change of filter (program iterates over list)
num_of_shots_free = 1
```

```
num_of_shots_450 = 1
num_of_shots_500 = 1
num_of_shots_630 = 1
num_of_shots_dark = 1

;delay between two subsequent image acquisitions on one filter position [s]
delay_free = 0
delay_450 = 0
delay_500 = 0
delay_630 = 0
delay_dark = 0
;delay after one complete capture sequence [s]
delay_sequence = 5 ;NOTE: when in alternating light source mode this adds up
    to 'light_src_warmup'
;max. number of cycles to run
cycles = 1
```

In the last block, the image size and position can be specified to limit the recorded area only to the area of the Hele-Shaw cell and therefore reduce the disk space of the individual images to a minimum. Along with this subfolder names for the images acquired at the different filter positions and the base name of the image files can be defined. Also there are options for the used type of time stamps given in `filename_style` and options for the log file name.

```
;position and size of image
pos_left = 1
pos_top = 360
size_width = 2400
size_height = 1346
;where to put in the output files (in the upper general output_folder)
output_folder = images ;string
;subdirectories for pictures of different wavelength. They are created in the
    images output_folder
output_folder_450 = 450_nm
output_folder_500 = 500_nm
output_folder_630 = 630_nm
output_folder_free = no_filter
output_folder_dark = dark
;output file basename, gets modified by process time
file_basename = topview_img_ ;this has to end with "_"
;filename style: "unixtime" or "processtime"
filename_style = unixtime
;name of log file
img_logfile = image.log ;string
;aperture, for logging purpose only
;aperture = 5.8 ;double
```

3.4.2 Image Processing

To process the acquired images, calculate the gap width of the Hele-Shaw cell and the concentration fields recorded during the observation a python script collection is provided on the evaluation computer. In the following an introduction into how to use the scripts is given.

How to run the processing script. To enable interaction with the plots, we want to run the scripts from the Spyder development environment. To launch Spyder open a terminal and navigate to the directory of the python scripts with `cd /Users/f59/Documents/Python_scripts/ltm_image_processing`. Then we need to activate an Python environment to load the appropriate Python packages by typing `source activate ltm_image_processing` and confirm this. Now you should see `(ltm_image_processing)` prepended to the command line. With this you can start Spyder with `spyder ltm_image_processing.py ltm_image_processing_cfg.py` simultaneously open the processing script `ltm_image_processing.py` and the script `ltm_image_processing_cfg.py`, which is used as the configuration file for the former script. To eventually run the processing script open the corresponding tab in the Spyder editor and press the green play button at the top or press F5.

How to set up the configuration script. The `ltm_image_processing_cfg.py` configuration script provides several options and parameters to determine the behavior of the image processing. In the following the options are described in the individual blocks of the script.

At first the task for the image processing has to be specified. The default task is always to calculate the spatially resolved gap width of the Hele-Shaw cell by invoking *Lambert Beers law* as described in section 3.2. This task is performed every time the processing script is executed and the corresponding output files are generated. Additionally the concentration fields can be calculated from the images of the observation measurement by setting `calculate_conc_fields` to `True`.

```
# Specification of the desired task:  
calculate_conc_fields = False
```

The next part gives options for the plots that are generated during the image processing. The first options are whether the plots should be saved and the other parameters specify the range of the colormaps to visualize the data. The initial guess for these parameters can be estimated from the initial condition of the experiment and the setup of the Hele-Shaw cell, but will probably need later adjustment to optimally present the data.

```
# Parameters for plots:  
save_gap_width_plot = True  
save_conc_field_plots = True  
# Specification of the colormap range for the plots:  
# For gap width in m and for concentration fields in mg/l
```

```
gap_vmin = 0.0005
gap_vmax = 0.002
conc_vmin = 0.08
conc_vmax = 0.3
```

Other necessary specifications are directories of the raw images. This structure assumes that the data of the calibration and observation measurement is contained in the same directory `common_dir_data` and also that the calibration measurements for pure water and the Brilliant Blue solution are contained in the same directory `calibration_dir`. For the exemplary directories given below the full path to the raw images of the pure water calibration then must have the structure `/Users/f59/Documents/Data/sample_data/experiment2017-01-07a/calibration_water/images/630_nm` and for the dark images accordingly with `dark` instead of `630_nm`. For the Brilliant Blue solution calibration this has to be `/Users/f59/Documents/Data/sample_data/experiment2017-01-07a/calibration_BB/images/630_nm` for the images taken with the band pass filter and `/Users/f59/Documents/Data/sample_data/experiment2017-01-07a/calibration_BB/images/dark` for the dark current images. In this example the structure for the raw images of the observation then would be `/Users/f59/Documents/Data/sample_data/experiment2017-01-07b/images/630_nm` and for the dark images `/Users/f59/Documents/Data/sample_data/experiment2017-01-07b/images/dark`. So make sure that you adapt the directories of your data to mimic this structure and then specify the correct paths.

```
# Directories of the data (has to be adapted):
common_dir_data = "/Users/f59/Documents/Data/sample_data"
calibration_dir = "experiment2017-01-07a"
calibration_backgrnd_subdir = "calibration_water"
calibration_BB_subdir = "calibration_BB"
observation_dir = "experiment2017-01-07b"
filter_wavelength = "630_nm"
```

The following part determines the output directories. These will then be contained in `/Users/f59/Documents/Data/sample_data/output/` for the given example. With `output_file_type` the data type of the output files can be specified that are generated along with the optional plots. These files then contain the data that is visualized in the plots and can be used for further evaluation.

```
# Determine output directories:
calibration_output_subdir = "gap_width"
observation_output_subdir = "concentration_fields"
observation_visualization_subdir = "visualization"
output_file_type = "hdf5_single_file" # either "hdf5", "hdf5_single_file" or
                                     "csv"
```

Here the general time format is specified that affects the file names of all the output files for the concentration fields. For example the file `conc_field_t_00060.png` is the png file of the concentration field plot for the measurement time of 60 minutes, if `time_unit=`

'minutes' was specified. As the values are round to the given time unit the value has to match the image acquisition time steps or otherwise the file names might not be unique and the output data gets partially overwritten.

```
# Parameters concerning the saved file names:  
time_unit = 'minutes'
```

Also the values for the extinction coefficient of Brilliant Blue at 630 nm and the concentration of the Brilliant Blue solution used for the gap width calibration gained by the measurements with the spectrometer have to be handed over to the processing script.

```
# Parameters for Lambert-Beer-Law (measurement Photometer):  
extinction_BB_630nm = 1.202 * 10**4 # in m2/kg  
conc_BB_calibration = 0.086572 # in g/l
```

To determine the region of the raw images, where the reference area for the image brightness is located the coordinates of the area corners have to be assigned to the following parameters. To get the values open a raw image and open it with GIMP. Use the cursor and hover over the wanted positions. The pixel values are shown in the lower left corner of the program window. Write down the pixel values for the upper left and lower right corner of the reference area.

```
# Coordinates of reference area for brightness correction (from gimp):  
ref_area_x1 = 2076  
ref_area_x2 = 2430  
ref_area_y1 = 340  
ref_area_y2 = 852
```

As for the image brightness reference area, coordinates have to be specified to crop the images to show only the interesting areas, namely the area of the glass plates. To get the coordinates repeat the process as for the reference area by opening a raw image with GIMP. Preferably this would be an image of the calibration measurements with pure water to identify the area of the glass plates.

```
# Coordinates of image area to cut (from gimp):  
cut_x1 = 70  
cut_x2 = 2028  
cut_y1 = 2  
cut_y2 = 1138
```

With this configurations completed, the image processing script `ltm_image_processing.py` is ready to be executed as described above.

4 Comprehension Check

The following questions and statements provide a basis to check whether you understood the previous chapters sufficiently well. When you are able to answer the questions and comment on the statements, you are prepared to continue with the experimental procedure.

- Explain the conceptual ideas on how to derive the *Navier Stokes equation*.
- Why can the *Navier Stokes equation* be simplified for the flow in porous media?
- Why is the fluid flow in Hele-Shaw cells analogue to the fluid flow in porous media?
- Do you understand the principle behind the dimensionless formulation of the governing equations and what is its benefit?
- Can you qualitatively explain *Taylor-Aris dispersion*?
- Explain the competing transport processes at the onset of the density-driven instability.
- Describe the temporal regimes of the density-driven instability.
- What are the two interpretations of the *Rayleigh number*? Can you explain them?
- Explain the experimental setup.
- Do you understand the measurement method to derive the concentration fields?
- Do you understand the equipment used in the experiments? Namely:
 - Hele-Shaw cell
 - Spectrometer
 - CCD-camera
 - Properties of Brilliant Blue

5 The Experiments

This chapter gives a detailed description of the tasks that have to be performed to prepare the experiments and run them. The following short description gives a summary and introduces the idea of the experiment.

This type of experiment is conducted with a bare Hele-Shaw cell, which means the narrow gap ($\leq 1\text{mm}$) between the glass plates is solely filled by de-ionized water or Brilliant Blue solution. The experiment is initialized with a homogeneous distribution of Brilliant Blue within the cell and an open upper edge. At this edge the unstable density gradient is established by evaporation of the water, leaving an increased concentration of Brilliant Blue. To balance the loss of water due to the evaporation, three inlets at the lower edge provide Brilliant Blue solution with the initial concentration. In this experiment the behavior is quite well understood and the phenomena as described in chapter 2 can be observed. Note that due to the slow process of evaporation, this experiment has to run at least for about 18 to 24 hours to get some beautiful results. Therefore this might introduce a day off, with respect to the practical course, depending on the general progress.

In the following the detailed steps to prepare and run the experiment are given in the respective section.

5.1 Bare Cell Experiment

Preparation

To get started with this experiment you need to prepare the materials first. Let's start with the assembly of the bare Hele-Shaw cell as described in the provided assembly guide. After you finished the assembly the cell has to be checked for leakages. For that put the cell in one of the provided plastic tubs and connect the inlet tube to a syringe filled with pure water. Fill the cell with the pure water, but leave a little space empty beneath the top edge of the glass plates, since the sealing tubes are still deforming slowly. Therefore, the volume of the gap still decreases and the water level in the cell rises. To observe this process measure the distance between the water level and the upper edge of the glass plates and do so 15 minutes later. After another 15 minutes check back if you can still observe a changing water table.

While the sealing tubes are settling you should start to prepare the Brilliant Blue solution needed for the calibration measurements and the experiment. For this get the 30000 mg/l base solution, the pipettes and the measurement flasks and dilute the base solution accordingly to receive a desired concentration. This concentration can be chosen within the range of 50 mg/l to 70 mg/l. The decision should be based on the following considerations. Higher concentrations lead to stronger density gradients as evaporation sets in and therefore leads to a faster process, but too high concentrations could lead to nearly optically opaque regions in the cell causing a bad measurement signal there. Lower concentrations typically produce better measurement signals, but also lead to a slower temporal development of the system. For the calibration and the experiment you need at least one liter of Brilliant Blue solution.

At this point you should be ready to start with the calibration measurements, if the cell did not show any leaking and the water table is stable.

Before transferring the cell onto the mount, this is a good point to measure the dimensions of the cells frame. These measurements are needed later to calculate the conversion from pixels to meters.

Calibration

Attach the water filled Hele-Shaw cell in front of the light source using the four provided screws. Ensure that the cell is only 1 cm to 2 cm away from the light source and that the cell is mounted completely parallel to the optical diffusor.

The next step is to understand the software to control the light source and the camera. For this refer to section 3.4.1 and adjust the settings in `adjust.ini`. It is recommended to keep a copy of that file, in case you mess something up completely. Note that the execution of the program can always be aborted by pressing CTRL + C, although it might take a while to quit.

You can check the acquired images in the respective output folder you have specified in the ini-file. While doing that you should also adjust the position of the camera, the focal point of the object lens and make sure that a brightness reference area (piece of paper in foil) is placed on the diffusor of the light source. The brightness reference area should be placed above the Hele-Shaw cell, when viewing from the perspective of the camera.

If you think you do understand how the control of the camera and the light sources work, you can start with the calibration measurements. Now, completely fill the cell with pure water that the water level is right at the upper edge of the glass plates as shown in the cell cross section depicted in Figure 5.1. Afterwards adjust the settings of the exposure for the 630 nm band pass filter and the aperture of the object lens such that the brightest regions of the cell in the produced images are at about 80% of the saturation of the camera chip. This means for the AVT Pike camera, which records with a bit depth of 16 bit, that the brightest regions must not exceed a gray value of 52400. This can be checked with the provided Matlab script `simple_image_explorer`. For that call `simple_image_explorer('PATH_TO_IMG_FILE')` in the Matlab terminal and use the 'Data Cursor' tool to get individual gray values. Note that these settings have to be adjusted under the conditions of the experiments and therefore the ambient lights have to be turned off.

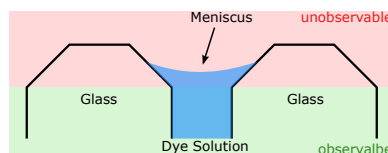


Figure 5.1: Cross section of the Hele-Shaw cell's upper region with the correct position of the meniscus of either pure water or Brilliant Blue solution for the calibration and the observation. Also shown are regions that are not directly observable by the CCD camera. Figure from [Kreyenberg \(2015\)](#).

When the everything is adjusted correctly you can adopt the values of `adjust.ini` to `image_acquisition.ini` and specify a unique output directory there and set `num_of_shots_630` and `num_of_shots_dark` to 100. Run the image acquisition.

Afterwards empty the Hele-Shaw cell by opening the valve and placing a empty beaker glass beneath the inlet tube. When the cell is empty fill a syringe with the prepared Brilliant Blue solution and rinse the cell from above. This is done by carefully injecting the solution into the gap and traversing the syringe over the whole width of the cell. This process should be repeated until the solution dripping out of the inlet tube isn't diluted by the previously contained pure water anymore. The next step is to completely fill the cell with the Brilliant blue solution from below to prevent air bubbles within the gap. Also fill the mariotte flask with the Brilliant Blue solution and attach it to the inlet tube. Adjust the height of the flask such, that the lower end of the straw is level with the upper edge of the cells glass plates. This might need to be adjusted to ensure that the level of the solution in the cell and the potential induced by the mariotte flask are in equilibrium. The meniscus has to be then again right at the upper edge of the glass plates (cf. Figure 5.1).

With this setting, again take 100 images by changing the output directory in `image_acquisition.ini` and running the `image_acquisition` script.

This are all the measurements needed to calculate the gap with of the Hele-Shaw cell in a spatially resolved manner. Note that since the evaporation at the upper edge sets right in after the cell is filled with the Brilliant Blue solution, the acquisition of the calibration images should not take too long as the experiment has essentially already started.

Observation

Now that the Hele-Shaw cell is filled with Brilliant Blue solution and the mariotte flask is connected to the inlet tube, evaporation sets in at the upper open edge of the cell. This process increases the Brilliant Blue concentration over time leading to density gradients that cause the phenomena we want to observe.

For this run the `image_acquisition` script with the according ini file, where you set a new output directory, `num_of_shots_630` and `num_of_shots_dark` back to 1. The values for `delay_sequence` and `cycles` should be set such that you take an image approximately every seven minutes and the product of the two parameters equates to the maximum duration planned for the experiment. Note that it is always possible to quit the image

acquisition before the script has iterated through all the cycles, therefore don't worry too much about the maximum time and just make sure that it runs longer than 24 hours.

Before you start the image acquisition make sure that you take the Brilliant Blue solution to the spectrometer lab to be able continue with the concentration determination while the experiment is running and put the "experiment running" sign at the outside of the door. Start the image acquisition and leave the laboratory.

Brilliant Blue Concentration Determination

While the experiment is running you can use the time to determine the exact concentration of the Brilliant Blue solution you prepared earlier. This is done in the laboratory with the spectrometer and the method described in section [3.3.2](#). Also a guide on how to use the spectrometer is provided right at the machine.

Since the maximum concentration the spectrometer can detect before the signal saturates is at about 25 mg/l, you need to dilute the Brilliant Blue solution accordingly. For this take the provided pipettes and the volumetric flasks and prepare at least 5 different samples. To get an idea of the error that is caused by the pipetting it is recommended that each of you creates several samples.

6 Evaluation

For the evaluation of the conducted experiments at least the following points should be covered in detail.

6.1 Qualitative evaluation of the image time series

To calculate the concentration fields for the acquired image time series execute the image processing script as described in section 3.4.2 and configure it such that the plots of the concentration fields are generated. To create a video from these plots use the program 'Zeitraffer', which is installed on the evaluation computer. The user interface should be somewhat self explanatory and you can adjust the the frames per second for the video output. A value of about 12 fps should give a good playback speed to give a interpretable presentation of the data.

With this video deduce a first qualitative description of the observed phenomena. While you are doing this you should, at least, discuss the following points and illustrate them with the corresponding concentration fields:

- Generally describe what you can see in the video and try to explain it with the concepts given in chapter 2.
- Which temporal regimes of the transient behavior can be seen in the video?
- Do the phenomena seem to appear as expected, or are there deviations? Are there ideas why the behavior could differ?
- What would you expect for different initial conditions i.e. a considerably lower and higher initial concentration of Brilliant Blue?
- Qualitatively discuss the influence of *Taylor-Aris dispersion* (see section 2.6.2) on the conducted observations.

6.2 Determination of the Critical Time and Wave Length

The next exercise is to determine the critical measures of the phenomena that are accessible with the obtained data. These measures are the critical values of the onset time t_{crit}

and the initial wave length λ_{crit} of the instability as introduced in section (2.7.4). For the critical time t_{crit} no accurate measurement is available and you have to derive the value from the observation image series and the calibration images taken with the Brilliant Blue solution filled Hele-Shaw cell. With the video and the concentration fields obtained as described in section 6.1, search for the onset of the density driven instability. With this identify the corresponding image in the raw data image set and get the time stamp of the file name. Also get the time stamp of the first image taken for the calibration measurement with the Brilliant Blue solution as this determines the start of the evaporation and calculate the elapsed time. The time stamps are given in UNIX time in micro seconds, which is the time passed since the 1 January 1970, 00:00:00 (in UTC). Shortly discuss the value and its uncertainty range.

The critical wave length λ_{crit} is determined by the examination of a concentration profile along the x-axis of the concentration field shortly after the onset of the instability. For this a profile near to the upper edge of the glass plates is taken by extracting the concentration values of only one pixel line of the concentration field. Make sure that you choose a time step for the extraction of the profile, where the density fingers are clearly visible, but no merging of the fingers, or only very little merging has occurred yet, since the initial spacing is conserved in this regime. With this get the number of the respective concentration field by simply counting the files by starting with 0.

For the extraction of the concentration profile use the provided Python script `extract_concentration_profile.py`, which is contained in the same directory as the processing script. Open the script in Spyder from the terminal by navigating to the respective directory and typing `spyder extract_concentration_profile.py`, or, if Spyder is already running, by using the graphical user interface to open the script. In the script you have to adapt the directories of the hdf5 file obtained from the image processing, the output directory, file name of the output csv file, the time step number of the chosen concentration field and the z-position to generate the concentration profile. The value of the z-position should be chosen such that it is close to the upper edges of the glass plates, but not too close since the signal tends to be very affected by strong noise. About 10 to 15 pixels should be a good start, but you probably have to adjust fine tune the value to get the best results. Run the script the same way as the image processing script by pressing the green 'play' button or by pressing the F5 key. The script generates an interactive plot of the concentration profile and writes values in the specified csv file. With this determine the value for λ_{crit} and discuss your method. Also extract the concentration maxima C_{max} to be able to determine the density difference $\Delta\rho$ of the initial phase. For the conversion from pixels to meters you can use the dimensions of the frame of the Hele-Shaw cell.

With the values of t_{crit} and λ_{crit} calculate the values for the parameters a and b as given by equation (2.57) and (2.58). The missing parameters for this calculation are accessible with the information given in chapter 2 and chapter 3 except for the dynamic viscosity of water μ that you have to look up elsewhere. While doing this calculation also include thoughts about the uncertainty range of the results and what you would expect for the values of the critical measures for different initial conditions.

6.3 Detailed investigation of the Temporal Regimes

The last task of the evaluation is to visualize the temporal evolution of the previously investigated concentration profile. The Python script `create_concentration_profile_time_series_plot.py` provides a tool to generate a time series plot of the concentration profile. Essentially the script stacks all the concentration profiles extracted from the image series in the direction of the temporal development.

As before, open the script in Spyder and configure the paths to the hdf5 file containing the data obtained by the image processing, the path and name of the output file and the z-position of the concentration profile. Run the script to create the plot and save it.

With this plot reconsider the classification of the temporal regimes you made earlier on the basis of the video. Do your earlier observations agree with the time series plot? What other behavior is visualized by the time series plot?

Bibliography

- Aris, R. (1956), On the dispersion of a solute in a fluid flowing through a tube, in *Proceedings of the Royal Society of London A: Mathematical, Physical and Engineering Sciences*, vol. 235, pp. 67–77, The Royal Society.
- Conrad, C. P., and P. Molnar (1997), The growth of RayleighTaylor-type instabilities in the lithosphere for various rheological and density structures, *Geophysical Journal International*, 129(1), 95–112, doi:10.1111/j.1365-246X.1997.tb00939.x.
- Davidson, O., and B. Metz (2005), Special report on carbon dioxide capture and storage, *International Panel on Climate Change, Geneva, Switzerland*, pp. 1–100.
- Diersch, H.-J., and O. Kolditz (2002), Variable-density flow and transport in porous media: approaches and challenges, *Advances in Water Resources*, 25(8), 899–944.
- Doering, C., and P. Constantin (1998), Bounds for heat transport in a porous layer, *J. Fluid Mech.*, 376, 263–296.
- Einstein, A. (1905), über die von der molekularkinetischen Theorie der Wärme geforderte Bewegung von in ruhenden Flüssigkeiten suspendierten Teilchen, *Annalen der Physik*, 322(8), 549–560.
- Ennis-King, J. P., L. Paterson, and others (2005), Role of convective mixing in the long-term storage of carbon dioxide in deep saline formations, *Spe Journal*, 10(03), 349–356.
- Fernandez, J., P. Kurowski, L. Limat, and P. Petitjeans (2001), Wavelength selection of fingering instability inside Hele-Shaw cells, *Physics of Fluids (1994-present)*, 13(11), 3120–3125.
- Fick, A. (1855), Ueber diffusion, *Annalen der Physik*, 170(1), 59–86.
- Howard, L. N. (1964), Convection at high rayleigh numbers, In *Applied Mechanics, Proceedings of 11th Congress of Applied Mathematics (ed. H. Görtler)*, p. 1109–1115.
- Kolditz, O., R. Ratke, H.-J. G. Diersch, and W. Zielke (1998), Coupled groundwater flow and transport: 1. Verification of variable density flow and transport models, *Advances in Water Resources*, 21(1), 27–46.
- Kreyenberg, P. J. (2015), *Experimental studies on evapo-induced density-driven flow in Hele-Shaw cells*, Institut für Umweltphysik, Universität Heidelberg, master thesis.
- National Center for Biotechnology Information, N. C. f. B. (2015), *Brilliant Blue FCF* C37H34N2Na2O9S3 - PubChem.

- Nield, D. A., and A. Bejan (1999), *Convection in porous media*, 2nd edition ed., Springer Science & Business Media.
- Riaz, A., M. Hesse, H. A. Tchelepi, and F. M. Orr (2006), Onset of convection in a gravitationally unstable diffusive boundary layer in porous media, *Journal of Fluid Mechanics*, 548(-1), 87, doi:10.1017/S0022112005007494.
- Roth, K. (2012), *Soil Physics. Lecture Notes.*, Institute of Environmental Physics, Heidelberg University, www.iup.uni-heidelberg.de/institut/forschung/groups/ts/students/sp.
- Roth, K. (2016), *Fundamentals of Environmental Physics. Lecture Notes.*, Institute of Environmental Physics, Heidelberg University, <https://shangrila.iup.uni-heidelberg.de:5101/sharing/8FRzRPIBE>.
- Saffman, P. G., and G. Taylor (1958), The penetration of a fluid into a porous medium or Hele-Shaw cell containing a more viscous liquid, *Proceedings of the Royal Society of London. Series A. Mathematical and Physical Sciences*, 245(1242), 312–329.
- Sharp, D. H. (1984), An overview of Rayleigh-Taylor instability, *Physica D: Nonlinear Phenomena*, 12(1), 3–18.
- Slim, A. C. (2014), Solutal-convection regimes in a two-dimensional porous medium, *Journal of Fluid Mechanics*, 741, 461–491.
- Van Dam, J. C., J. N. M. Stricker, and P. Droogers (1992), Inverse method for determining soil hydraulic functions from one-step outflow experiments, *Soil science society of America journal*, 56(4), 1042–1050.
- Wooding, R. A., S. W. Tyler, and I. White (1997a), Convection in groundwater below an evaporating salt lake: 1. Onset of instability, *Water Resources Research*, 33(6), 1199–1217.
- Wooding, R. A., S. W. Tyler, I. White, and P. A. Anderson (1997b), Convection in groundwater below an evaporating salt lake: 2. Evolution of fingers or plumes, *Water Resources Research*, 33(6), 1219–1228.